Mineral Petrol (2008) 93: 153–183
DOI 10.1007/s00710-007-0227-z
Printed in The Netherlands

Mineralogy and Petrology

U-Pb zircon ages and geochemical data for the Monumental Granite and other granitoid rocks from Aswan, Egypt: implications for the geological evolution of the western margin of the Arabian Nubian Shield

F. Finger[1], **W. Dörr**[2], **A. Gerdes**[3], **M. Gharib**[4], **M. Dawoud**[5]

[1] Department of Materials Engineering and Physics, University of Salzburg, Salzburg, Austria
[2] Institute for Mineralogy, University of Frankfurt, Frankfurt a.M, Germany
[3] Institut für Geowissenschaften, Justus-Liebig Universität, Giessen, Germany
[4] Geology Department, Faculty of Science, Helwan University, Cairo, Egypt
[5] Geology Department, Faculty of Science, Menoufiya University, Shabin El-Kom, Egypt

Received July 2 2007; Accepted November 18 2007; Published online May 5 2008

Editorial handling: J.G. Raith

Summary

U-Pb zircon ages and geochemical data are presented for Pan-African granitoid rocks sampled in the area of Aswan, Egypt, close to the inferred boundary between the Saharan Metacraton and the Arabian Nubian Shield. The sample set includes tonalitic gneisses as well as undeformed, post-tectonic tonalites to granites (Aswan Tonalite, Monumental Granite, High-Dam Granite, Saluja-Sehel Granite). A tonalitic gneiss with a volcanic-arc type geochemical signature gave a zircon age of 622 ± 11 Ma, while the Aswan Tonalite and the Monumental Granite intruded at 606 ± 1 and 606 ± 2 Ma, respectively. The age of the High-Dam Granite was constrained at 595 ± 11 Ma. These data imply that the western parts of the Arabian Nubian Shield were accreted to the Saharan Metacraton prior to 606 Ma in the area of Aswan, most probably between 630 and 615 Ma.

The Aswan Tonalite, the Monumental Granite and the High-Dam Granite have high Zr, Y and LREE contents and can be classified as A-type granitoids. Furthermore they are

Correspondence: F. Finger, Department of Materials Engineering and Physics, University of Salzburg, Hellbrunnerstraße 34, A-5020 Salzburg, Austria
e-mail: Friedrich.Finger@sbg.ac.at

rich in K, Ba, Sr, Ti and P, thus displaying affinities to shoshonitic magma series. The shoshonitic A-type plutonism at Aswan constitutes an exceptional feature within the Late Neoproterozoic granite terrain of the Arabian Nubian Shield. It may contain components from an enriched, subduction-modified mantle wedge, that had developed beneath the western margin of the Arabian Nubian Shield in response to the eastward subduction of the Mozambique ocean. It is suggested that slab break-off provided the tectonothermal conditions for a post-collisional melting of this subduction-modified mantle wedge.

Introduction

Additionally to its importance as antique building stone, the so-called Monumental Granite at Aswan in southern Egypt has received considerable geological interest during the past years, since it seems to represent an important time marker for large-scale tectonic processes that occurred along the contact between the Arabian Nubian Shield and the Saharan Metacraton (Abdelsalam et al., 2002). Based on field observations, Gindy and Tamish (1998) have proposed that the granite magma formed and intruded as a consequence of collisional crustal thickening, which resulted from the docking of the Neoproterozoic island-arc-type crust of the Arabian Nubian Shield to the Palaeoproterozoic Saharan Metacraton. The country rocks, metasediments, orthogneisses, amphibolites and metagabbros, record the magmatic and sedimentary history of the pre-collisional crust and were metamorphosed during the collision stage.

The main objective of the present study is to provide precise and reliable age data for the Monumental Granite by means of the single-grain ID-TIMS U-Pb zircon dating method, in order to link the chain of events with an absolute time scale. Furthermore, zircons from two other post-collisional granitoid rocks of the area and for an orthogneiss were geochronologically investigated, using a combination of ID-TIMS and Laser ICP-MS methods. These new data help to resolve the timing of collision between the Arabian Nubian Shield and the Saharan Metacraton, which until now was just very crudely bracketed. Based on the geochemistry and typology of the granitic rocks at Aswan we present a model that attempts to describe the tectono-magmatic evolution of the western margin of the Arabian Nubian Shield during the Late Neoproterozoic.

Geological background

The bedrocks of Egypt belong to two fundamentally different tectonic provinces, the Arabian Nubian Shield in the east, and the Saharan Metacraton in the west (Fig. 1). Whereas the Saharan Metacraton represents Palaeoproterozoic, high-grade metamorphic basement, the Arabian Nubian Shield consists of Neoproterozoic, mainly low- to medium-grade metamorphic, arc-related successions with intercalated ophiolite remnants (e.g., Kröner, 1985; Stern and Hedge, 1985). As a consequence of the convergence of East- and West Gondwana and the closure of the Mozambique ocean, this juvenile crust accreted against the Saharan Metacraton by the end of the Proterozoic (Kusky et al., 2003) and was intruded at that time by a large number of granitoids (Greiling et al., 1994). The supposed accretion zone follows the Nile near Aswan (Gindy and Tamish, 1998). According to the tradi-

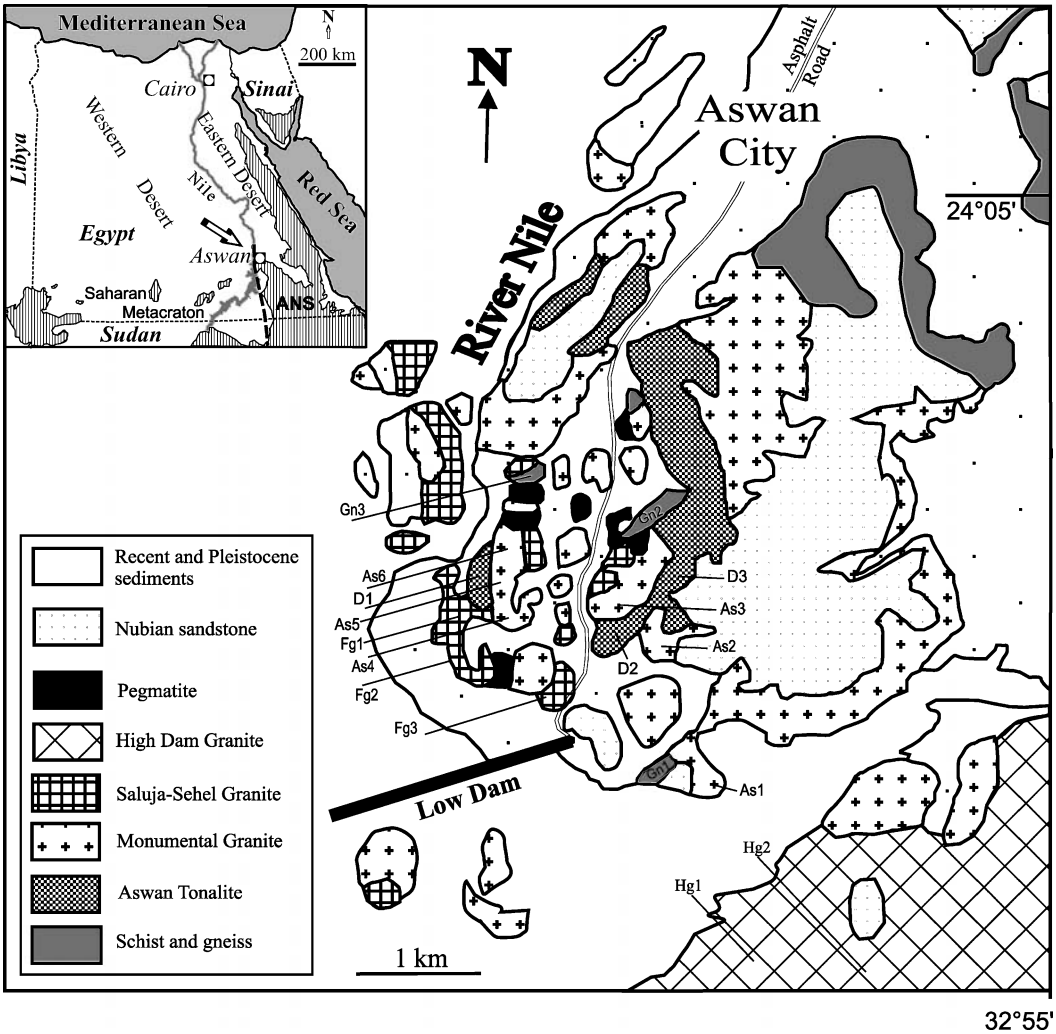

Fig. 1. Geological sketch map of the area of Aswan (after Gindy and Tamish, 1998) with sample locations of the present study. Inset shows the exposed Precambrian of Egypt and the presumed plate boundary (*dashed line*) between the Arabian Nubian Shield (ANS) and the Saharan Metacraton after Dixon and Golombek (1988)

tional view (Dixon and Golombek, 1988), the plate boundary runs from there in a southerly direction into Sudan (Fig. 1). However, this has been critically debated in Schandelmeier et al. (1993). Based on research in northern Sudan these authors considered that the actual suture may perhaps be farther to the west.

On the Egyptian side the areal extent of the cratonic crust of the Saharan Metacraton is also ill-defined, which is not only a matter of limited exposure: Sultan et al. (1994) have shown that a reliable separation of Neoproterozoic and Palaeoproterozoic rocks on the basis of field criteria (degree of metamorphism, lithology, etc.) is very difficult, if not impossible. Based on U-Pb zircon dating, Sultan et al. (1994) proposed a Neoproterozoic formation age for orthogneisses west of the Nile (e.g., at Gebel Um Shagir), which were previously believed to belong to the Saharan Metacraton.

Unlike some previous workers (e.g., El Gaby et al., 1990), Gindy and Tamish (1998) considered the deformed, amphibolite-facies schists and gneisses near Aswan not as metacratonic crust, but as remnants of an accretionary prism consisting of Neoproterozoic material of the Arabian Nubian Shield thrust onto the Saharan Metacraton. They proposed that this crustal thickening event caused melting at depth, generating the granitic magmas which intruded in the Aswan area. Pb isotope data indicate a contribution of pre-Neoproterozoic crustal material to these granitoids (Sultan et al., 1992).

Based on previous mapping (Gindy, 1956), four types of post-collisional, largely undeformed, granites are distinguished in the Aswan area (Gindy and Tamish, 1998):

1) A coarse-grained, porphyritic, fairly mafic ''granodiorite''. According to our data this rock is rather a tonalite than a granodiorite and we refer to it as Aswan Tonalite in the following.
2) The famous coarse-grained, pink to red, porphyritic Monumental Granite with rapakivi texture in places.
3) The fine-grained, mostly pink Saluja-Sehel Granite.
4) The so-called High-Dam Granite, which is a coarse-grained, mostly non-porphyritic biotite granite.

The regional distribution of these granitoids is shown in Fig. 1. Contact relationships indicate that the Aswan Tonalite is the oldest intrusion. Then the Monumental Granite intruded and after that the fine-grained Saluja-Sehel Granite (Gindy and Tamish, 1998). These three build up a composite pluton south of Aswan City. The High-Dam Granite is considered the youngest intrusion (Gindy and Tamish, 1998). It forms by far the largest body and is located further south with prominent outcrops near the so-called ''High-Dam'' of the Nile reservoir (slightly outside of the map area on Fig. 1).

Several authors have suggested that all four plutonic units are comagmatic, with the magmas being derived from the same or a similar source, but having undergone varying degrees of magmatic differentiation during ascent (Ragab et al., 1978; Noweir et al., 1990; Gindy and Tamish, 1998).

Previous geochronological work

Due to its undeformed nature the Monumental Granite was always considered as a Late Neoproterozoic rock and not as part of the metamorphic Proterozoic basement. This was confirmed by early Rb-Sr whole-rock dating which provided ages of between ca. 570 and 610 Ma (Leggo, 1968; Hashad et al., 1972; Ragab et al., 1978). With one exception (Hashad et al., 1972), the $^{87}Sr/^{86}Sr$ initial ratio of the granite was estimated to be ~ 0.703 (see also Stern and Hedge, 1985). The significantly higher value of 0.709 given in Hashad et al. (1972) is enigmatic and possibly in error.

Abdel Monem and Hurley (1980) analysed six zircon fractions from the Monumental Granite and obtained variably discordant (partly reversely discordant) data points with U-Pb ages ranging between ca. 500 and 700 Ma. The ^{207}Pb-^{206}Pb age of the oldest and least discordant fraction (710 Ma; ^{238}U-^{206}Pb age: 684 Ma;

^{235}U-^{207}Pb age: 688 Ma) is often cited as representing the formation age of the granite (e.g., Noweir et al., 1990). However, Stern and Hedge (1985) analysed two zircon fractions of the Monumental Granite which, although both discordant (U-Pb ages around 500 Ma), showed correspondingly lower ^{207}Pb-^{206}Pb ages. The discordia age of these two fractions (upper intercept at 594 ± 4 Ma) was considered as the approximate granite formation age by Stern and Hedge (1985).

An orthogneiss belonging to the metamorphosed roof was dated at 634 ± 4 Ma (protolith age) by Sultan et al. (1994). Since this zircon age of Sultan et al. (1994) appears reliable (upper intersect age from 3 just slightly discordant data points), it provides a strong argument that the Monumental Granite did not intrude prior to ~ 634 Ma.

Samples and petrographic data

From three of the four major granite types of the area (Aswan Tonalite, Monumental Granite, High-Dam Granite) representative, large samples ($\sim$10 kg) have been taken for zircon dating (D1, As5, and Hg2; see sample locations in Fig. 1). Fifteen ca. 2 kg samples were collected for petrographic and geochemical work. Additionally, a large sample of a tonalitic gneiss from the metamorphic roof has been taken for zircon dating (Gn1 in Fig. 1).

The coarse-grained, porphyritic Monumental Granite has a relatively uniform modal composition with $\sim$35–38% K-feldspar (strongly perthitic), $\sim$10% plagioclase (An 10–15), 31–35% quartz, 7–10% biotite, 4–5% hornblende. It can be termed a Hbl-Bt (syeno)granite in terms of the Streckeisen nomenclature.

The Aswan Tonalite consists of 35–40% plagioclase, 15–25% quartz, $\sim$20% biotite and $\sim$20% hornblende. It contains hardly any K-feldspar (<2%), at least in those three samples studied here. According to the Streckeisen nomenclature the rock should be called a Bt-Hbl tonalite.

The samples of High-Dam Granite are coarse-grained and equigranular. They are distinguished from the Monumental Granite by a lack of hornblende. Compared to the samples of Monumental Granite, they contain more plagioclase (20–23% albite-oligoclase) and less quartz (23–26%). The rock has $\sim$10% modal biotite and can be classified as a biotite granite.

The tonalitic gneiss used for dating consists of $\sim$25% plagioclase (oligoclase-andesine), 35% quartz, 25% hornblende (partly altered to tremolite-actinolite) and 10% biotite. It has a coarse gneissose texture.

The accessory minerals magnetite, sphene, zircon and apatite can be found in all four granitoid rocks. In addition, the Monumental Granite hosts relatively large allanite (up to 1 mm) and occasional monazite crystals.

U-Pb zircon dating

Zircons

The zircons in the Aswan Tonalite, the Monumental Granite and the tonalitic gneiss are similar regarding their size and morphology. They commonly form large (200–300 μm), elongate euhedral crystals with length/width ratios of 3–6. The

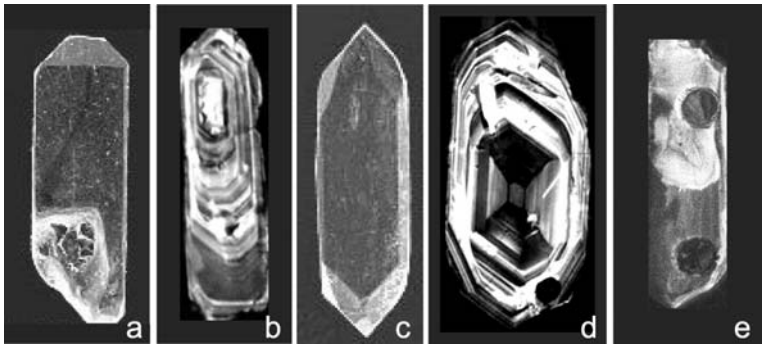

Fig. 2. Morphologies and CL zoning patterns of zircons from Monumental Granite (**a**, **b**) and High-Dam Granite (**c**, **d**). Figure 2e shows a CL image of a core-bearing zircon from the tonalitic gneiss; round craters are LA-ICP-MS analyses spots 12 and 15, see Table 2

dominant crystal faces are (100) and (101), whereas (211) and (110) are subordinate or missing (Fig. 2a and b). Cracks and inclusions are abundant. In the tonalitic gneiss some rounded zircon grains are also present.

The zircons from the High-Dam Granite are less elongate and have larger (211) faces combined with the (101) pyramid (Fig. 2c and d). They commonly show facets of the (110) prism additional to the (100) prism, which is generally dominant.

Cathodoluminescence (CL) images of the zircons mostly show pronounced magmatic oscillatory zoning (Fig. 2b and d). Sometimes resorbed inner domains can be observed that might be inherited. Such ''cores'' are relatively more abundant in the tonalitic gneiss sample (Fig. 2e) and the High-Dam Granite, but can also be seen occasionally in the zircons from the Monumental Granite and the Aswan Tonalite. A detailed description of the accessory zircon crystals in the rocks (morphology, CL images) is given by Gharib and Dawoud (2005).

Analytical details

Samples for isotope dilution – thermal ionisation mass spectrometry (ID-TIMS) were processed at the IGL (Institut für Geowissenschaften und Lithosphärenforschung) of the University of Giessen, Germany, using standard mineral separation techniques. These include sieving before concentration of heavy minerals by heavy liquid (methylene iodide) and magnetic-separation with a Frantz isodynamic separator. Zircons with the size of 120–350 µm were handpicked from the >1.6 A non-magnetic fraction of the heavy mineral separate. After abrasion with pyrite for 10 h (Krogh, 1982) the grains were washed with HNO_3 and 2 N HCl in an ultrasonic bath. Zircons were weighed and loaded with 24 N HF and a mixed $^{205}Pb/^{235}U$ spike into small Savillex^{TM} vials, which were then placed into a Parr bomb (Parrish, 1987). After dissolution at 180 °C for 62 h and subsequent evaporation to dryness at ca. 80 °C on a hotplate, the sample was converted into chloride by adding 0.2 ml 3 N HCl. Chemical separation of Pb and U on 100 µl columns (ion-exchange resin AG 1×8, 100–200 mesh) followed the method of Krogh (1973). The U and Pb isotope ratios were obtained using a Finnigan MAT 261 mass

spectrometer in static multicollector mode with simultaneous ion counting of ^{204}Pb. All isotopic ratios were corrected for mass fractionation (1.1 ± 0.2‰/a.m.u), blank (app. 5 pg for single zircon) and initial lead, using the Stacey and Kramers (1975) model Pb composition. The U-Pb data were calculated using the program PBDAT (Ludwig, 1988), the isotope ratios were plotted using Isoplot (Ludwig, 2000), with error ellipses reflecting 2σ uncertainty. The concordia curves are plotted with decay-constant errors.

LA-ICP-MS analyses were performed at the Mineralogical Institute of the University of Frankfurt, Germany, using a Thermo-Finnigan Element II sector field ICP-MS coupled to a New Wave UP213 ultraviolet laser system. A teardrop-shaped, low volume laser cell was used to enable sequential sampling of heterogeneous grains during time resolved data acquisition (see also Janousek et al., 2006). Zircon grains mounted in resin blocks and polished to half their thickness were analysed for ^{202}Hg, ^{204}Hg, ^{204}Pb, ^{206}Pb, ^{207}Pb, ^{208}Pb, ^{232}Th, ^{235}U and ^{238}U in peak jumping mode using a laser spot-size of 30 µm. Each analysis consisted of approximately 20 s background acquisition followed by 35 s data acquisition. The ^{204}Pb signal interferes with the ^{204}Hg isotope that occurs together with ^{202}Hg in the argon carrier gas. The precise detection of ^{204}Pb was therefore dependent on accurate monitoring of Hg. A common-Pb correction based on the calculated ^{204}Pb and a model Pb composition (Stacey and Kramers, 1975) was carried out where necessary. The necessity of the correction is judged on whether the corrected ^{207}Pb/^{206}Pb lies outside of the internal errors of the measured ratios. Raw data were corrected for background signal, common Pb, laser-induced elemental fractionation, instrumental mass discrimination, and time-dependent elemental fractionation of Pb/Th and Pb/U using an Excel® spreadsheet program. Reported errors (1σ on ratios, 2σ on ages) were propagated with the reproducibility (1 s.d.) of the GJ-1 standard ($n = 12$) over the entire session, which were 0.6% and 0.7% for the ^{207}Pb/^{206}Pb and ^{206}Pb/^{238}U ratios, respectively. Concordia diagrams (2σ error ellipses) and concordia ages (95% confidence level) were produced using Isoplot/Ex 2.49 (Ludwig, 2000). For further details on analytical protocol and data processing see Gerdes and Zeh (2006).

Results

Table 1 and Fig. 3 show the results of ID-TIMS analyses of single zircon grains. Several concordant data points constrain the crystallization ages of the Monumental Granite and the Aswan Tonalite at 605.9 ± 2.2 Ma and 605.5 ± 1.4 Ma, respectively. Both plutonic rocks are seemingly of identical age and cogenetic, as has also been proposed by Gindy and Tamish (1998), based on field relationships. Our data provide no significant evidence for the presence of inherited zircon components in the Monumental Granite, however, this may be due to biased sampling (only clear, elongate euhedral crystals were analysed). The zircon grain 2703 from the Monumental Granite (see Table 1) has experienced slight lead loss but shows a Pb-Pb age of 602 ± 10 Ma in accordance with the calculated concordia age. In the Aswan Tonalite, zircon grains 2635 and 2638 are interpreted to contain a minor inherited component and were not used for the calculation of the crystallization age (see Fig. 3).

Table 1. *ID-TIMS U-Pb isotopic data and ages of zircons from the investigated granitoids*

Sample													Ages (Ma)		
	Weight µg	U ppm	Pb r. ppm	Pb i. ppm	$^{206}Pb/^{204}Pb^*$	$^{207}Pb/^{235}U$	$\pm 2\sigma\%$	$^{206}Pb/^{238}U$	$\pm 2\sigma\%$	$^{207}Pb/^{206}Pb$	$\pm 2\sigma\%$	Cor.	$^{206}Pb/^{238}U$	$^{207}Pb/^{235}U$	$^{207}Pb/^{206}Pb$
Monumental Granite (As5)															
2701	8	119	12.8	4.91	166	0.8214	± 2.59	0.09854	± 1.53	0.06046	± 2.02	0.63	606 ± 9	608 ± 15	620 ± 44
2699	9	482	50.5	4.19	721	0.8231	± 0.82	0.09862	± 0.42	0.06053	± 0.70	0.53	606 ± 3	609 ± 5	622 ± 15
2700	10	156	17.6	1.66	588	0.8082	± 1.48	0.09755	± 1.03	0.06009	± 1.03	0.72	600 ± 6	601 ± 9	607 ± 22
2698	11	514	52.3	4.37	732	0.8213	± 1.15	0.09785	± 0.39	0.06087	± 1.07	0.36	602 ± 2	608 ± 7	634 ± 23
2702	12	38.5	5.06	1.08	236	0.8319	± 4.76	0.09822	± 3.26	0.06143	± 3.35	0.71	604 ± 19	614 ± 28	654 ± 72
2705	11	90	9.5	2.39	246	0.8160	± 2.50	0.09745	± 1.53	0.06073	± 1.91	0.64	600 ± 9	606 ± 15	629 ± 41
2703	9	588	57.6	2.02	1737	0.7884	± 0.59	0.09536	± 0.34	0.05997	± 0.47	0.60	587 ± 2	590 ± 4	602 ± 10
High-Dam Granite (Hg2)															
2713	19	268	24.5	3.67	451	0.8374	± 1.23	0.09556	± 0.34	0.06355	± 1.17	0.31	588 ± 2	618 ± 7	726 ± 25
2712	12	447	44.5	4.91	551	0.8156	± 0.77	0.09430	± 0.33	0.06273	± 0.68	0.46	581 ± 2	606 ± 5	699 ± 15
2708	11	223	20	7.89	168	0.7359	± 2.41	0.08559	± 0.77	0.06236	± 2.25	0.37	529 ± 4	560 ± 14	686 ± 48
2709	16	338	28	4.64	358	0.6452	± 1.07	0.07517	± 0.41	0.06225	± 0.97	0.43	467 ± 2	506 ± 6	682 ± 21
Aswan tonalite (D1)															
2633	11	224	26.5	1.96	722	0.8214	± 1.11	0.09895	± 0.67	0.06020	± 0.86	0.63	608 ± 4	609 ± 7	611 ± 19
2632	9	174	18.1	3.08	364	0.8188	± 1.75	0.09862	± 1.03	0.06022	± 1.37	0.62	606 ± 6	607 ± 11	611 ± 30
2639	13	428	47.6	3.36	796	0.8187	± 0.54	0.09843	± 0.31	0.06032	± 0.43	0.61	605 ± 2	607 ± 3	615 ± 9
2648	8	522	66.1	0.98	3253	0.8156	± 0.68	0.09818	± 0.40	0.06025	± 0.54	0.61	604 ± 2	606 ± 4	612 ± 12
2635	14	851	105.6	3.05	1712	0.8238	± 0.62	0.09783	± 0.31	0.06107	± 0.53	0.51	602 ± 2	610 ± 4	641 ± 11
2638	15	75.6	8.2	3.54	151	0.8454	± 2.92	0.10042	± 1.26	0.06105	± 2.51	0.52	617 ± 8	622 ± 18	641 ± 54
Tonalitic gneiss (Gn1)															
2719	12	111	14.7	0.72	1122	1.0343	± 1.52	0.11505	± 1.02	0.06520	± 1.10	0.69	702 ± 7	721 ± 11	781 ± 23
2716	14	1166	277	1.84	4338	0.9697	± 0.25	0.10985	± 0.17	0.06402	± 0.18	0.68	672 ± 1	688 ± 2	742 ± 4
2717	11	1544	800	31.7	317	0.8316	± 0.63	0.09892	± 0.21	0.06097	± 0.57	0.44	608 ± 1	615 ± 4	638 ± 12
2718	15	139	13.2	2.15	395	0.7882	± 1.31	0.09420	± 0.78	0.06068	± 1.03	0.62	580 ± 4	590 ± 7	628 ± 22
2715	9	375	24.5	4.99	267	0.4425	± 1.39	0.05357	± 0.83	0.05991	± 1.07	0.64	336 ± 3	372 ± 5	600 ± 23

Errors are quoted at 2 sigma level. * Corrected for mass fractionation (1.12 ± 0.18‰ per a.m.u.), ^{205}Pb-spike contribution and analytical blank. *Pb r.* Radiogenic lead; *Pb i.* initial common lead; *Cor* correlation coefficient of $^{207}Pb/^{235}U$ to $^{206}Pb/^{238}U$ errors

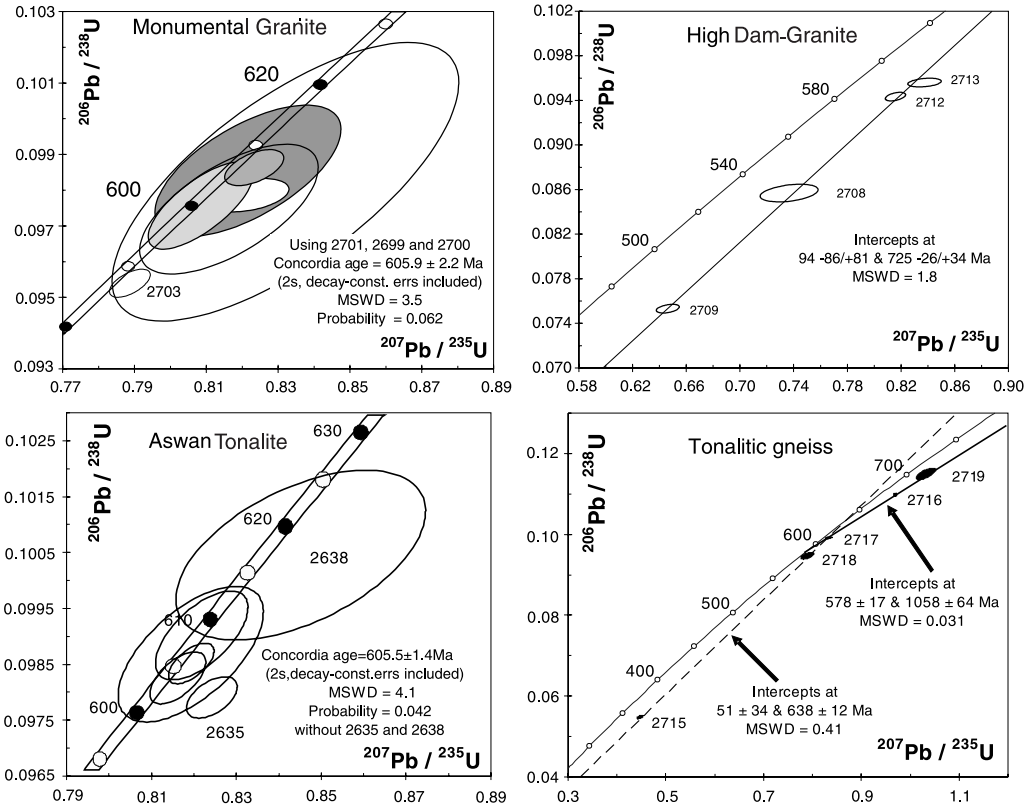

Fig. 3. Concordia diagrams showing ID-TIMS U-Pb isotopic data for zircons from the four investigated samples

In contrast to the Aswan Tonalite and the Monumental Granite, ID-TIMS zircon dating of the High-Dam Granite and the tonalitic gneiss provided only discordant data points (Fig. 3). Data for the High-Dam Granite are alligned along a discordia chord with an upper intercept at 725 Ma. However, the variable Pb-Pb ages of the single zircons and the lower intercept age of the discordia far above zero (94 Ma) cast doubt on whether this 725 Ma date is of any geological significance. As to the tonalitic gneiss, the distribution of data points in the concordia diagram indicates a disturbance of the U-Pb system by a combination of lead loss and inheritance. The relatively low Pb-Pb ages of three of the five zircons (600, 628 and 638 Ma) are interpreted to indicate that the magmatic formation age of the gneiss protolith was not much older than that of the Monumental Granite. These zircons (2715, 2717 and 2718 in Table 1) define a discordia (MSWD = 0.41) with an upper intercept age of 638 ± 12 Ma (Fig. 3).

For both rocks, independent geochronological information has been derived by means of the LA-ICP-MS method (Table 2 and Fig. 4). Using CL images for orientation, laser spots were placed into oscillatory zoned magmatic zircon domains apparently free of inclusions, cracks or cores. A well-defined discordia chord has been obtained for the High-Dam Granite, with an upper intercept age of 595 ± 11 Ma. Data points show that the zircons in the High-Dam Granite obviously were affected by severe recent lead loss, which is certainly one reason for

Table 2. *Laser ablation ICP-MS U, Pb and Th data of zircon grains from the investigated granitoids*

Name (spot)	$^{207}Pb^a$ (cps)	U^b (ppm)	Pb^b (ppm)	Th^b/U	Isotopic ratios[c] $^{206}Pb/^{204}U$	$^{206}Pb/^{238}U$	1σ (%)	$^{207}Pb/^{235}U$	1σ (%)	$^{207}Pb/^{206}Pb$	1σ %	Rho[c]	Ages $^{207}Pb/^{235}U$	$\pm 2\sigma$ (Ma)	$^{206}Pb/^{238}U$	$\pm 2\sigma$ (Ma)	$^{207}Pb/^{206}Pb$	$\pm 2\sigma$ (Ma)	Conc. (%)
Tonalitic gneiss (Gn1)																			
I-A11	23424	347	37	0.50	53657	0.1006	0.8	0.8416	1.1	0.0607	0.7	0.78	620	13	618	10	627	28	99
I-A12	21419	712	74	0.45	86885	0.0993	0.9	0.8249	1.2	0.0603	0.8	0.73	611	14	610	10	614	34	99
I-A13	38838	552	61	0.58	46452	0.0994	1.0	0.8350	1.2	0.0609	0.7	0.80	616	15	611	12	637	32	96
I-A15	53145	361	47	0.39	9478	0.1199	1.0	1.0437	1.2	0.0632	0.8	0.79	726	18	730	14	714	32	102
I-A16	54416	804	92	0.55	194558	0.1060	0.8	0.8936	1.1	0.0611	0.7	0.74	648	14	649	10	644	31	101
I-A17	32620	454	52	0.68	170945	0.0990	1.0	0.8295	1.2	0.0608	0.6	0.87	613	14	609	12	631	25	96
I-A18	22921	314	36	0.70	22882	0.1024	0.9	0.8597	1.3	0.0609	0.9	0.73	630	16	628	12	636	38	99
I-A19	42079	592	66	0.51	82083	0.1032	1.0	0.8668	1.3	0.0609	0.7	0.82	634	16	633	13	637	32	99
I-A20	32539	467	55	0.63	6489	0.1048	0.9	0.8763	1.2	0.0607	0.8	0.72	639	15	642	11	627	35	102
I-A21	104848	936	106	0.45	22297	0.1012	0.9	0.8446	1.3	0.0605	0.9	0.69	622	16	622	11	622	41	100
I-A22	22035	213	24	0.42	11985	0.0979	0.8	0.8081	1.4	0.0599	1.2	0.56	601	17	602	10	600	50	100
I-A23	19704	285	31	0.47	25414	0.1036	0.9	0.8612	1.2	0.0603	0.7	0.78	631	15	636	12	614	32	104
I-A24	15534	178	18	0.35	12962	0.1005	1.0	0.8350	1.5	0.0603	1.0	0.70	616	18	617	13	613	45	101
I-A25	47312	679	77	0.34	14413	0.1044	1.1	0.8945	1.5	0.0621	1.1	0.70	649	20	640	14	678	47	94
High-Dam Granite (Hg2)																			
I-A26	198660	2100	182	1.40	253	0.0625	0.7	0.5101	1.4	0.0592	1.2	0.49	419	12	391	5	573	54	68
I-A27	107109	2734	150	1.32	862	0.0345	3.5	0.2794	3.7	0.0587	1.0	0.96	250	18	219	15	556	46	39
I-A28	117292	1788	180	1.47	1487	0.0743	1.4	0.6115	1.5	0.0597	0.6	0.91	485	15	462	13	591	27	78
I-A29	96009	1435	168	1.24	3086	0.0930	0.8	0.7556	1.2	0.0589	0.9	0.67	571	13	574	9	563	38	102
I-A30	159084	2842	147	1.92	501	0.0248	4.1	0.2041	4.2	0.0597	0.9	0.98	189	16	158	13	593	39	27
II-A1	105876	1505	185	1.29	3464	0.0957	1.2	0.7938	1.7	0.0602	1.1	0.75	593	20	589	15	610	47	97
II-A2	129271	1970	212	1.27	1670	0.0820	1.1	0.6731	1.3	0.0596	0.7	0.83	523	14	508	11	588	32	86
II-A3	188759	3364	209	1.59	728	0.0391	2.3	0.3201	2.3	0.0594	0.4	0.99	282	13	247	11	582	16	42

(*continued*)

Table 2 (*continued*)

Name (spot)	^{207}Pb[a] (cps)	U[b] (ppm)	Pb[b] (ppm)	Th[b]/U	Isotopic ratios[c] $^{206}Pb/^{204}U$	$^{206}Pb/^{238}U$	1σ (%)	$^{207}Pb/^{235}U$	1σ (%)	$^{207}Pb/^{206}Pb$	1σ %	Rho[c]	Ages $^{207}Pb/^{235}U$	$\pm 2\sigma$ (Ma)	$^{206}Pb/^{238}U$	$\pm 2\sigma$ (Ma)	$^{207}Pb/^{206}Pb$	$\pm 2\sigma$ (Ma)	Conc. (%)
II-A4	115685	3718	82	1.19	183	0.0127	4.7	0.1035	4.9	0.0590	1.5	0.95	100	10	82	8	566	65	14
II-A5	93952	1122	132	1.34	686	0.0874	1.0	0.7221	1.2	0.0599	0.7	0.79	552	13	540	10	601	32	90
II-A6	125694	1920	226	1.22	9777	0.0926	0.7	0.7628	0.9	0.0598	0.5	0.82	576	10	571	8	595	22	96
II-A7	156183	3610	137	1.73	278	0.0192	7.0	0.1560	7.1	0.0591	1.0	0.99	147	21	122	17	570	44	21
II-A8	206845	2467	285	1.75	1414	0.0644	1.3	0.5363	1.4	0.0604	0.6	0.92	436	13	402	11	618	24	65
Monumental Granite (As5)																			
II-A9	125044	2262	197	0.94	776	0.0712	2.8	0.5790	3.0	0.0589	1.1	0.93	464	28	444	25	565	50	79
II-A10	125411	2061	254	0.98	1191	0.0937	1.6	0.7699	2.0	0.0596	1.1	0.82	580	23	578	19	588	49	98
II-A11	117918	1936	138	0.25	7374	0.0703	2.2	0.5781	2.9	0.0596	1.8	0.77	463	26	438	19	590	80	74
II-A12	17970	479	57	0.65	706	0.1016	1.7	0.8575	2.3	0.0612	1.6	0.74	629	29	624	21	646	67	97
II-A13	15785	432	51	0.68	17245	0.0995	0.8	0.8335	1.7	0.0608	1.6	0.45	616	21	611	10	631	67	97
II-A14	48296	739	74	0.28	6060	0.0989	0.8	0.8253	1.6	0.0605	1.5	0.46	611	20	608	9	623	63	98
II-A15	24023	344	32	0.68	176	0.0745	1.5	0.6157	2.2	0.0600	1.6	0.69	487	21	463	14	602	68	77
II-A16	12913	166	17	0.40	546	0.0926	0.9	0.7772	1.8	0.0609	1.6	0.49	584	21	571	10	635	68	90
II-A17	13043	189	20	0.36	1420	0.1014	0.7	0.8535	1.6	0.0611	1.5	0.43	627	20	622	9	642	64	97
II-A19	28399	437	48	0.66	2495	0.0987	0.7	0.8245	1.2	0.0606	1.0	0.61	611	15	607	9	625	41	97
II-A20	51818	812	89	0.81	8639	0.0947	0.7	0.7821	1.2	0.0599	1.0	0.61	587	14	584	9	599	42	97
II-A21	54812	867	99	0.85	42080	0.0983	0.8	0.8068	1.2	0.0595	0.9	0.66	601	14	605	9	586	38	103

[a] Within-run background-corrected mean ^{207}Pb signal in counts per second

[b] U and Pb content and Th/U ratio were calculated relative to reference zircon GJ-1 and are accurate to approximately 10%

[c] Corrected for background, mass bias, laser induced U-Pb fractionation and common Pb (if detectable, see analytical method) using Stacey and Kramers (1975) model Pb composition. $^{207}Pb/^{235}U$ calculated using $^{207}Pb/^{206}Pb/(^{238}U/^{206}Pb \times 1/137.88)$. Errors are propagated by quadratic addition of within-run errors (1SE) and the reproducibility of reference zircon GJ-1 (1SD)

[d] Rho is the error correlation defined as $err^{206}Pb/^{238}U/err^{207}Pb/^{235}U$

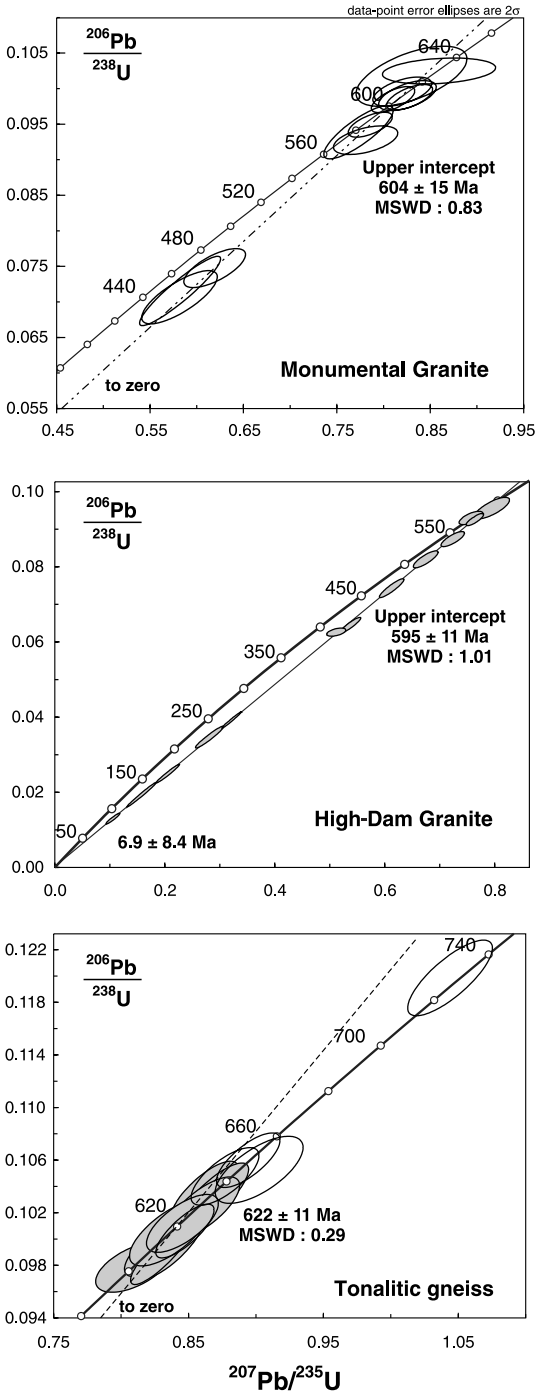

Fig. 4. Concordia diagrams showing LA-ICP-MS U-Pb isotope data for zircons from the Monumental Granite, the High-Dam Granite and the tonalitic gneiss

the discordant ID-TIMS ages. There is a notable positive correlation between the degree of discordancy and the U content (Table 2). The in part extremely high U contents (up to 3700 ppm) probably caused radioactive lattice damage and lead loss in such crystal domains. On the other hand, the ID-TIMS data indicate a significant inherited component (probably <900 Ma), which is not seen in the

LA-ICP-MS data set. This may be because core domains with inherited appearances in the CL images were systematically avoided during LA-ICP-MS dating. There was no point in targetting these cores for laser analyses, as their size was generally below that of the laser beam, and they appeared heterogenous and often metamict.

Zircons from the tonalitic gneiss analysed by LA-ICP-MS provided a cluster of concordant ages between 600 Ma and 650 Ma. One larger inherited core (Fig. 2e) yielded a concordant age of ~730 Ma. The data clearly show that the magmatic formation age of the rock must be between 600 and 650 Ma. However, the wide variation of single point ages, which do not all overlap within error, implies that some are influenced by slight lead loss or inheritance. It is difficult, however, to quantify these effects and several model solutions are possible. Assuming that the entire variation is caused by recent lead loss, then the crystallization age of the magmatic zircons would be represented by the mean Pb-Pb age (ca. 640 Ma). However, a critical re-examination of the measured grains using backscatter electron (BSE) images gives reason to assume that the three oldest data points with U-Pb ages of between 640 and 650 Ma are influenced by inherited cores that were marginally hit by the laser. The mean Pb-Pb age of the other points (622 ± 11 Ma) is therefore taken as the best estimate for the magmatic formation age of the tonalitic gneiss.

LA-ICP MS data obtained for zircons from the Monumental Granite (Fig. 4) show that the method provides results in good agreement with the ID-TIMS data. The upper intercept of a discordia chord defined by 12 single point analyses provides an age of 604 ± 15 Ma.

Geochemistry and granite typology

Granitoid groups

Representative geochemical analyses for the granitoid rocks of the Aswan area are listed in Table 3. The Harker diagrams in Fig. 5 include some additional data (this study – sample locations see Fig. 1; three analyses from Gindy and Tamish (1998), and four analyses of orthogneisses from Sultan et al. (1994)). Samples of Aswan Tonalite, Monumental Granite, High-Dam Granite, Saluja-Sehel Granite and orthogneisses (tonalitic to granitic) are shown with different symbols. It can be seen from the diagrams that these granitoid groups have distinct geochemical features:

The Saluja-Sehel Granite samples all have high SiO_2 (73–76 wt.%). They are slightly peraluminous and of high-K nature (Fig. 5). A distinctive feature of this granite are the high Rb and Th contents.

The Aswan Tonalite, the Monumental Granite and the High-Dam Granite (with the exception of one analysis given in Gindy and Tamish, 1998) can be described as metaluminous with mol $Al_2O_3/CaO + Na_2O + K_2O$ (A/CNK) ratios <1, and as high-K to shoshonitic according to the nomenclature of Pecerillo and Taylor (1976). The Aswan Tonalite samples are characterized by intermediate SiO_2 contents of 58–64 wt.% and show extremely high concentrations of some trace elements (TiO_2: 1–2.5 wt.%, P_2O_5: 0.6–1.4 wt.%, Ba: 1000–1800 ppm, Zr: 450–900 ppm, Y: ~60 ppm and Nb: ~50 ppm).

Table 3. *Geochemical analyses for the granitoid rocks from Aswan: (a, b) Monumental Granite. (c, d) Aswan Tonalite. (e) Saluja-Sehel Granite. (f) High-Dam Granite. (g, h) Tonalitic gneiss. Analyses by standard XRF methods at the University of Salzburg as described in Janousek et al. (2006). Major elements in wt.%, trace elements in ppm. LOI = Loss on ignition. Sample locations see Fig. 1*

Sample	a As5	b As6	c D1	d D3	e Fg2	f Hg2	g Gn1	h Gn3
SiO_2	70.48	71.80	58.93	63.50	72.58	68.50	52.49	53.00
TiO_2	0.52	0.60	2.11	1.23	0.25	0.50	1.80	2.12
Al_2O_3	12.80	13.59	12.40	13.50	14.16	15.20	10.83	11.40
Fe_2O_{3tot}	3.32	3.20	10.09	7.47	1.40	2.09	10.20	12.01
MnO	0.06	0.04	0.16	0.15	0.04	0.06	0.14	0.14
MgO	0.61	0.40	2.35	1.33	0.31	0.49	5.80	4.42
CaO	2.26	1.70	5.81	4.00	1.05	1.81	9.25	9.77
Na_2O	3.21	3.35	3.07	3.37	3.32	3.75	2.16	2.39
K_2O	4.75	4.90	1.97	3.17	5.14	5.65	2.51	1.11
P_2O_5	0.27	0.20	1.04	0.57	0.07	0.15	0.28	0.25
LOI	1.31	0.71	1.49	0.86	1.39	0.97	3.90	2.90
Total	99.59	100.49	99.42	99.15	99.71	99.17	99.36	99.51
A/CNK	0.88	0.98	0.70	0.83	1.09	0.98	0.47	0.50
F	638	432	1026	962	282	246	725	808
Cl	131	118	363	240	98	89	284	273
Sc	8	3	18	17	4	3	28	30
V	32	31	154	94	24	32	304	293
Cr	11	14	60	52	7	21	151	197
Co	4	4	23	14	3	4	36	36
Ni	6	6	18	13	3	4	43	57
Cu	20	18	35	39	14	19	23	18
Zn	75	61	162	159	33	66	85	132
Rb	105	97	78	64	183	128	89	10
Sr	211	185	493	357	122	467	245	273
Y	43	20	54	60	27	34	25	31
Zr	386	335	585	911	190	355	165	173
Nb	27	23	45	50	15	22	20	22
Ga	20	21	23	23	19	21	18	17
Cs	7	5	3	4	6	6	<3	<3
Ba	952	896	1056	1751	716	1571	284	152
La	109	63	55	64	47	47	13	16
Ce	273	153	123	170	112	117	37	46
Nd	101	51	85	110	45	53	28	32
Pb	21	15	10	11	18	26	5	4
Th	25	10	5	7	26	8	<3	<3
U	4	<3	<3	<3	7	4	<3	<3

The seven Monumental Granite samples all plot within a narrow SiO_2 range of 70–73 wt.%. With reference to some trace elements like P, Zr, La, Ce, and Nd, which occur in relatively high concentrations, they cover distinct vari-

ation fields that do not or hardly overlap with the other felsic granitoid groups (Fig. 5).

Three of the four samples of High-Dam Granite have an SiO_2 content of between 68 and 70 wt.% SiO_2, whereas the analysis given in Gindy and Tamish (1998) is significantly more felsic with 76 wt.% SiO_2. All High-Dam Granite samples are characterized by a particularly high K_2O content of >5 wt.%. Another distinctive feature are high Pb concentrations (Fig. 5).

The orthogneiss group shows a wide chemical variation (SiO_2: 52–75 wt.%) and includes high-K and low-K granitoids (Fig. 5). The mafic samples are meta-

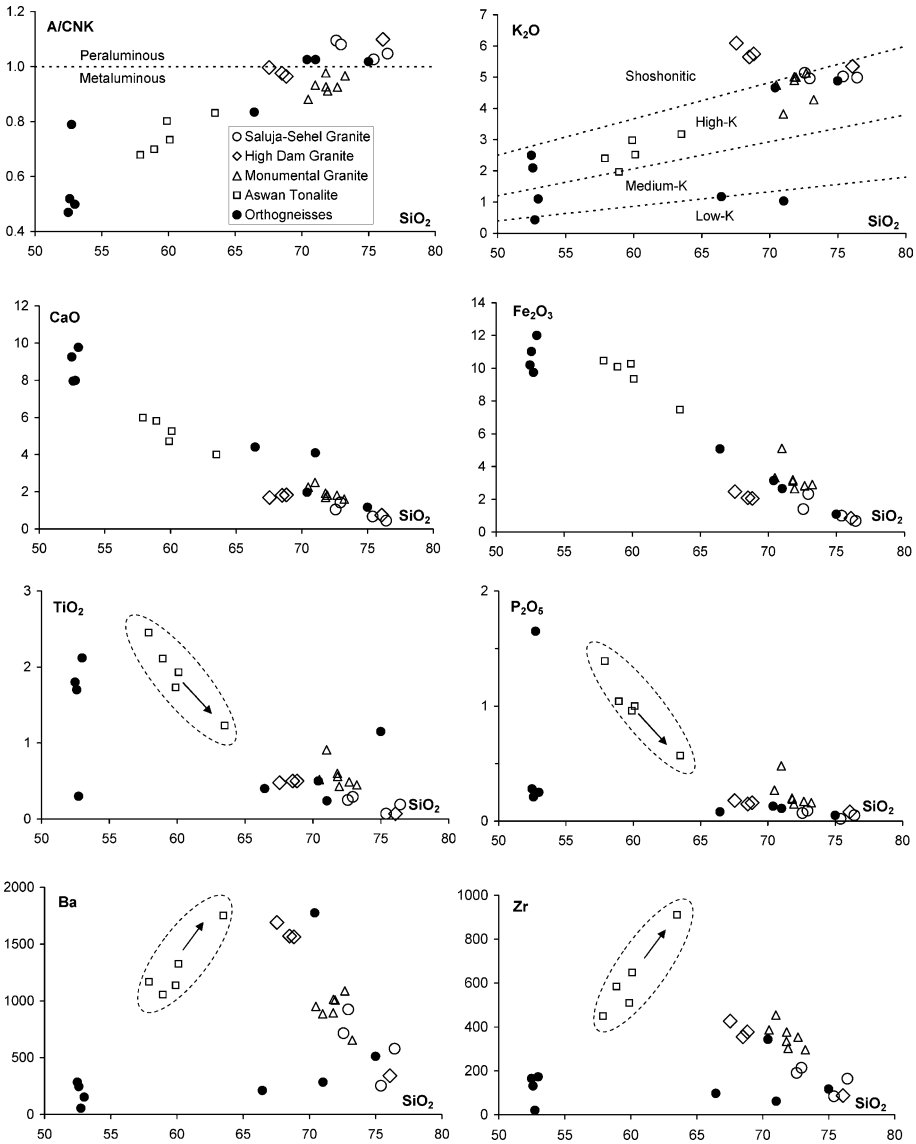

Fig. 5. Harker diagrams for major and trace elements illustrating the geochemical features of the different granitoid groups from Aswan. Characteristic features and trends mentioned in the text are indicated by ellipses and lines

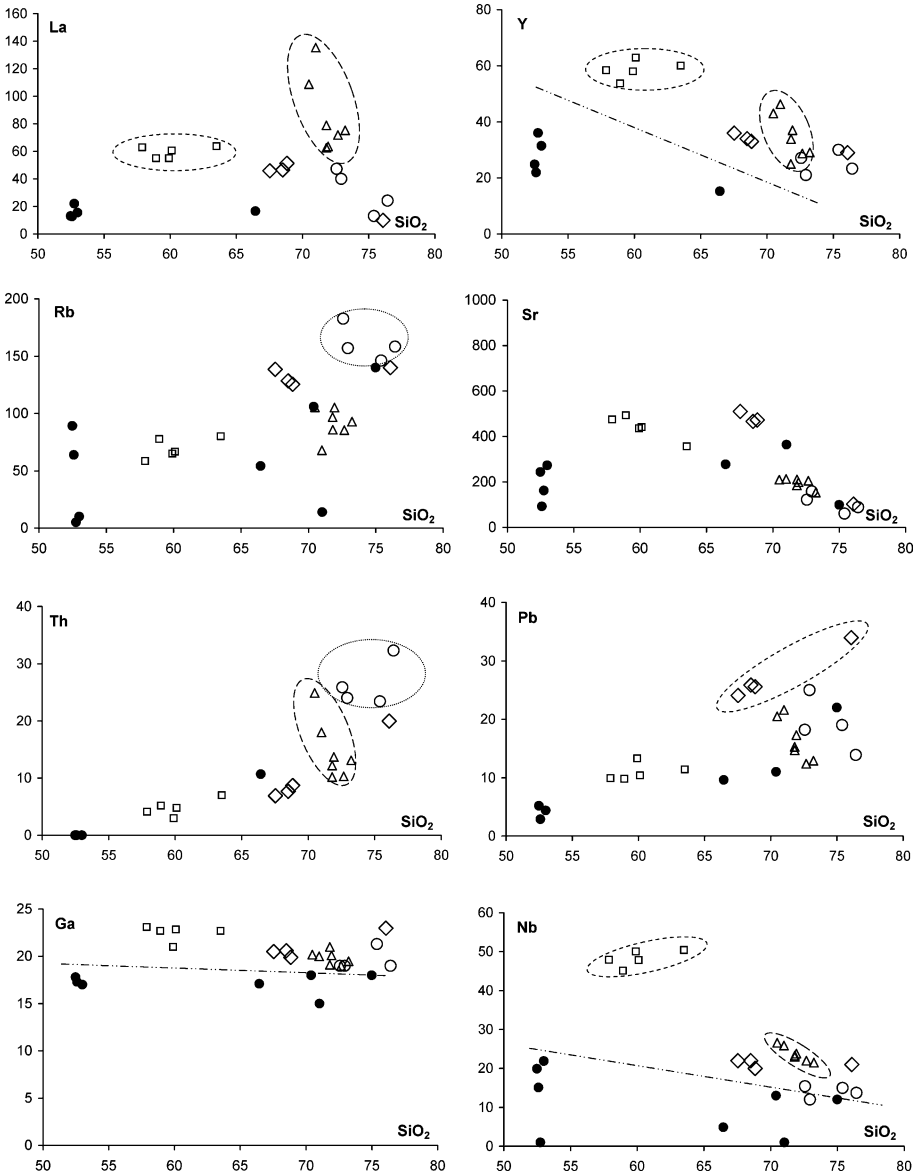

Fig. 5 (*continued*)

luminous, the felsic orthogneisses are slightly peraluminous. Trace element versus SiO_2 covariations show that the orthogneisses can be distinquished from the Aswan Tonalite, the Monumental Granite and the High-Dam Granite by systematically lower Nb, Y and Ga contents (see dashed lines in Fig. 5) and (with one exception) lower Ba, Zr and LREE contents.

Inferred sources and processes

According to its relatively small geochemical variation for most elements, the Monumental Granite is interpreted to represent a pristine magma that was little

modified by fractional crystallization during its ascent. The special geochemical features seen in the Monumental Granite (high Ti, Ba, Nb, LREEs, Zr and P) are thus most likely source-related. Some local magmatic accumulation of accessory minerals (in particular allanite and zircon) is indicated by the expanded trends for La, Th and Zr (Fig. 5).

A much larger internal variation can be seen within the Aswan Tonalite, regarding both major elements (CaO: 4–6 wt.%, Fe_2O_3: 7–11 wt.% and MgO 1–3 wt.%), as well as trace elements (TiO_2 1–2.5 wt.%, P_2O_5: 0.6–1.4 wt.%, Zr 450–900 ppm, Sr: 300–500 ppm, Ba: 1000–1800 ppm). Much of this variation can be explained in terms of successive fractionation of the liquidus mineral assemblage plagioclase + hornblende + apatite + (titano)magnetite and residual melt during magma ascent (i.e., a fractionation of exactly those minerals which can be considered as ''early magmatic'' also from thin section observations). Those tonalite samples which are particularly rich in P and Ti, etc. may therefore represent magmatic cumulates enriched in the above mentioned liquidus minerals, whereas the more felsic samples of the tonalite suite may represent evolved residual melt. The increase of Zr with SiO_2 (Fig. 5) indicates an incompatible behavior of this element in the Aswan Tonalite and rules out speculations that the rocks could be a cumulate facies of the adjacent Monumental Granite. The incompatible behavior of Zr is often observed in high-temperature granitoids (Chappell et al., 1998; Miller et al., 2003) and results from the high solubility of Zr in such magmas (Watson and Harrison, 1983). Using the equations of Watson and Harrison (1983), it can be estimated that the Aswan Tonalite had a temperature of in excess of 900 °C on the liquidus. Although geochemical modifications by fractional crystallization probably have occurred during magma ascent we may conclude from the variations seen in the Harker diagrams that both the primary magma and the magma source of the Aswan Tonalite were already particularly enriched in elements like Ti, P, Nb, Zr, LREEs, Y (HREEs), Ba and Sr.

For the High-Dam Granite more data would be needed to derive valid conclusions about the processes of magma evolution. The SiO_2-rich analysis given in Gindy and Tamish (1998) indicates that some differentiation by fractional crystallization is likely to have occurred. However, as stated previously, the less felsic samples of High-Dam Granite resemble the Monumental Granite with their high Zr, La, Ce, Ba and Sr contents. We therefore interprete that the Aswan Tonalite, the Monumental Granite and the High-Dam Granite contain components from the same type of source, although the data distribution in Harker diagrams (lack of well-defined coherent general trends e.g., for Sr, Ce, Pb and Rb with the SiO_2 – Fig. 5) do not favour a derivation of all three granitoid units from one parental magma simply by fractional crystallization.

Judging from their peraluminous A/CNK ratios and their significantly higher Rb and Th contents, the Sajula Sehel granites are derived from a different magma source. The limited variation of Rb and Th does not suggest that the enrichment of these elements occurred through fractional crystallization during magma ascent. Apparently, different parental magmas were able to form in the upper mantle/lower crustal region below Aswan, implying the availability of several kinds of fertile sources.

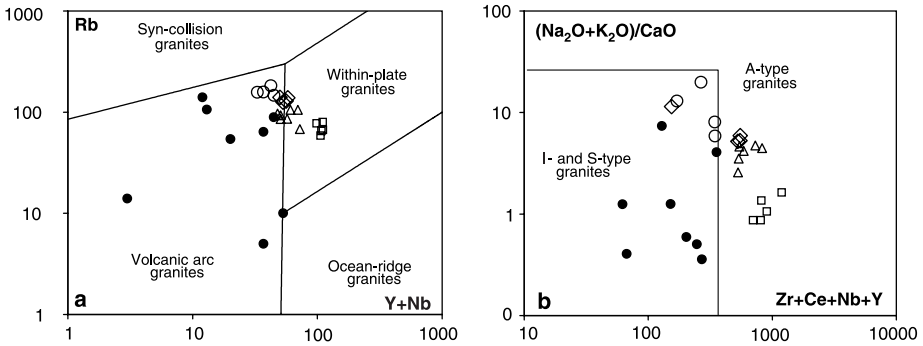

Fig. 6. Granite discrimination diagrams after Pearce et al. (1984) (**a**) and Whalen et al. (1987) (**b**) with plots of the granitoid rocks from Aswan

Using the common criteria for the subdivision of granites into ''types'', the orthogneisses and the Saluja-Sehel Granite can be classified as I-type (Chappell and White, 1974) or volcanic-arc-granites (Pearce et al., 1984), whereas the Aswan Tonalite, the High-Dam Granite and the Monumental Granite exhibit affinities to A-type granites (Whalen et al., 1987) or within plate granites (Pearce et al., 1984), due to their high contents of HFS elements (Fig. 6). We therefore summarize the Aswan Tonalite, the High-Dam Granite and the Monumental Granite in the following as the ''Aswan A-type granites''.

I-type granites can form through fractionation from mantle-derived, LILE-enriched basaltic melts in subduction settings (Pearce et al., 1984), or from remelting of mafic to intermediate igneous lower crust (Chappell and White, 1974; Clemens and Vielzeuf, 1987). Whereas the former scenario may be more appropriate for the orthogneisses of the Aswan area (especially the more mafic ones), the post-tectonic felsic Saluja-Sehel Granite may better match a model of remelting of (island-arc-type) lower crust.

Two main possibilities are discussed in the literature for the formation of A-type granites. The first is derivation through fractionation from basaltic parental melts that formed in an enriched mantle region (Pearce et al., 1984; Bonin, 1992). The second is high-T melting of restitic lower crust (Whalen et al., 1987). The latter model has originally been developed for silicic granites in the Lachlan Fold Belt, Australia, enriched in Zr and other HFS elements relative to the I-type granites of this area (Collins et al., 1982). The Aswan A-type granites are different from these Australian A-types 1) in that fairly mafic tonalitic A-type magmas are present and 2) in showing distinctly higher contents of Sr, Ba, Ti and P. Therefore, we hold the view that the A-type magmas at Aswan contain a significant component from an enriched (metasomatized) upper mantle region. The geochemistry of the Aswan A-type granites (high Zr and LREEs combined with high K, Sr, Ba, Ti and P) bears affinities to so-called ''shoshonitic'' magmas, for which a derivation from (phlogopite-bearing) enriched mantle is mostly assumed (e.g., Fitton et al., 1991; Hawkesworth et al., 1995; Wilson et al., 1997). Crucial for a petrogenetic interpretation of the A-type granites at Aswan is that they seem to be geochemically unique within the Late Neoproterozoic granitoid terrain of the Arabian Nubian Shield, as will be shown in the next section, and that they are situated near the suture with the Saharan Metacraton.

Comparison of the granitoids at Aswan with other granitoids in Egypt

The Arabian Nubian Shield is characterized by a particular abundance of granitoids. About 50% of the basement is made up of granitoid rocks (Stern and Hedge, 1985). These form a large number of individual intrusive complexes of variable size. Modern geochemical data do exist for several of these plutonic complexes and can be used for comparison (regarding the data base used in this study see Table 4).

Traditionally, the granitoids of the Arabian Nubian Shield are subdivided into two main age groups (El-Ramly and Akaad, 1960):

1) the older grey granites, which are variably deformed and sometimes also known as ''synorogenic granites'' (El Gaby, 1975) or G1 (Hussein et al., 1982). Their intrusion ages are between 610 and 850 Ma (Stern and Hedge, 1985; Hassan and Hashad, 1990; Kröner et al., 1990).
2) the younger pink and red granites, which are essentially undeformed, post-tectonic granites, with intrusion ages of ca. 600–550 Ma (Stern and Hedge, 1985; Hassan and Hashad, 1990). These granites are also known as ''post-orogenic granites'' in the Egyptian literature (El Gaby, 1975).

Table 4. *Geochemical data base for Late Neoproterozoic granitoid rocks from the Arabian Nubian Shield, used for this study*

Older granites	
Wadi El Sheikh	Gharib and Obeid (2004)
Abu El Hassan	Dawoud (1995)
Umm Gheig	El-Sayed et al. (2002)
Abu Marwa, Umm Rus, Fawakhir, Abu Ziran, Umm Had, Kadabora	El-Mahallawi (1989)
Orthogneisses Hafafit area	Kröner et al. (1994)
W. El Ghuzah, G. Semna, G. El-Gidami, W. Abu Zawil	Ahmed and El-Mahallawi (1995)
G. Umm Taghir, W. Umm Anab	Ahmed and El-Mahallawi (1995)
Kab Amiri	Moghazi (2002)
Sibai Central Gneisses	Bregar et al. (2002)
Wadi Shait	El-Mahallawi (1995)
Younger granites	
Abu El Hassan	Dawoud (1995)
Iqna	El-Metwally (1997)
Umm Gheig	El-Sayed et al. (2002)
Abu Marwa	El-Mahallawi (1989)
Ras Barud, Gebel El Dob, G. El-Aradiya, G. Umm Gidri	Ahmed and El-Mahallawi (1995)
G. Miskeat, W. Abu Diwan	Ahmed and El-Mahallawi (1995)
Kab Amiri	Moghazi (2002)
Sibai	Bregar et al. (2002)
Gabal Saint Katherine	Gharib and Obeid (2004)
Wadi Dib, Zargat Naam, Nigrub El Tahtani, St. Katherina	Ghoneim et al. (1999)
Gebel Ghareb, Wadi Lithey, Gebel El Zeit, Gebel El Sibai	Hassan and Abu Anbar (1997)
Gebel El Shayeb, Gebel Musa, West Safaga	Hassan and Abu Anbar (1997)
Mount Gharib	Abdel Rahman and Martin (1990)
Bakriya ring complex	El-Sayed et al. (2004)
Wadi Kareim-Wadi El Atshan, Gebel Um Khors	Hassan and Abu Anbar (1997)
Gebel Um Shaghir, Gebel El Atawi	Hassan and Abu Anbar (1997)

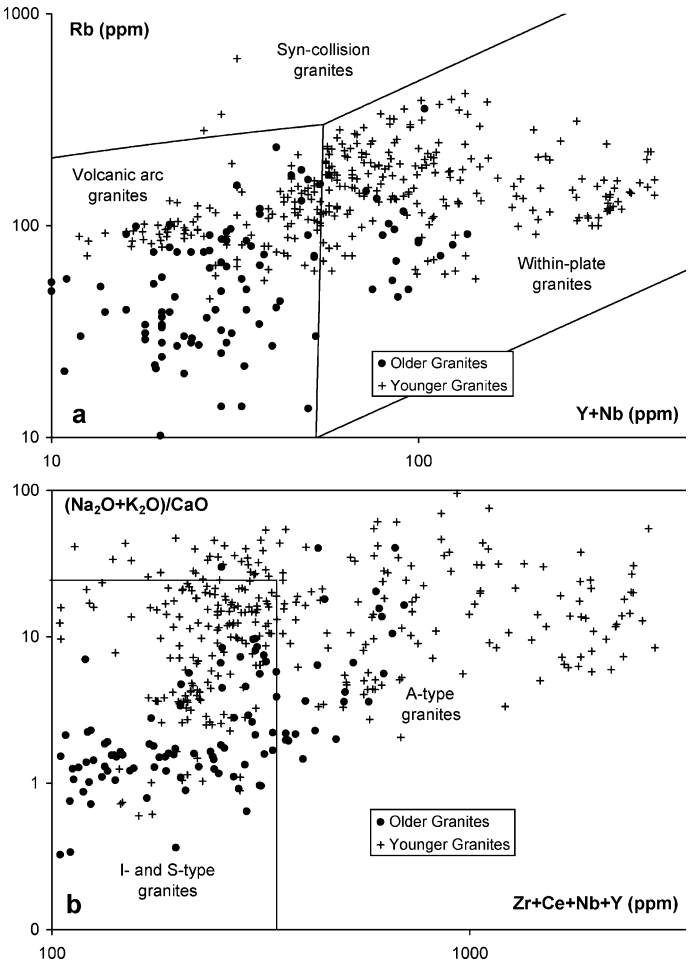

Fig. 7. Distribution of the older grey granites and the younger pink and red granites of the Arabian Nubian Shield in the granite discrimination diagrams of Pearce et al. (1984) (**a**) and Whalen et al. (1987) (**b**). Data base see Table 4

The older grey granites are mostly considered to represent magmas that formed above subduction zones, during the island-arc stage of crustal evolution (Hassan and Hashad, 1990). They comprise mainly low- to medium-K, often hornblende-bearing, I-type tonalites and granodiorites. In the Rb vs. Y + Nb granite discrimination diagram of Pearce et al. (1984) they preferentially plot in the Rb-poor sector of the volcanic arc granite (VAG) field (Fig. 7). A few felsic variants of the older grey granites have affinities to A-type or within-plate granites (Dawoud, 1995; Gharib and Obeid, 2004). Considering their age and composition, the orthogneisses at Aswan can probably be regarded as metamorphosed equivalents of the older grey granites (e.g., Figs. 6 and 7).

The younger pink and red granites have partly I-type, but more often A-type signatures (Fig. 7). The A-types among them include hypersolvus granites as well as peralkaline variants and they often form characteristic intrusive structures, so-called ring complexes (Hassan and Hashad, 1990). In the Rb vs. Y + Nb diagram of Pearce et al. (1984), the younger pink and red granites plot in the Rb-rich sector of the VAG field and in the within-plate granite (WPG) field (Fig. 7). The abundance of A-type (within-plate) granites and the scarcity of S-type (syn-collision) granites is a characteristic feature of the entire Late

Neoproterozoic granite terrain of the Arabian Nubian Shield. The I-type (VAG) variants among the younger granites are often interpreted as remolten island-arc type lower crust (e.g., Moghazi, 2002), whereas for the A-type (WPG) variants melting of restitic (melt depleted) lower crust has been suggested (Jackson et al., 1984) or, in particular for the ring complexes, formation from an enriched lithospheric mantle source in an extensional tectonic regime (El-Sayed et al., 2004).

With respect to their post-tectonic setting, their HFSE-rich compositions and their partly hypersolvus nature and pink colour (Monumental Granite), the Aswan A-type granites naturally display similarities with the younger pink and red granites of the Arabian Nubian Shield (Noweir et al., 1990). However, it is impor-

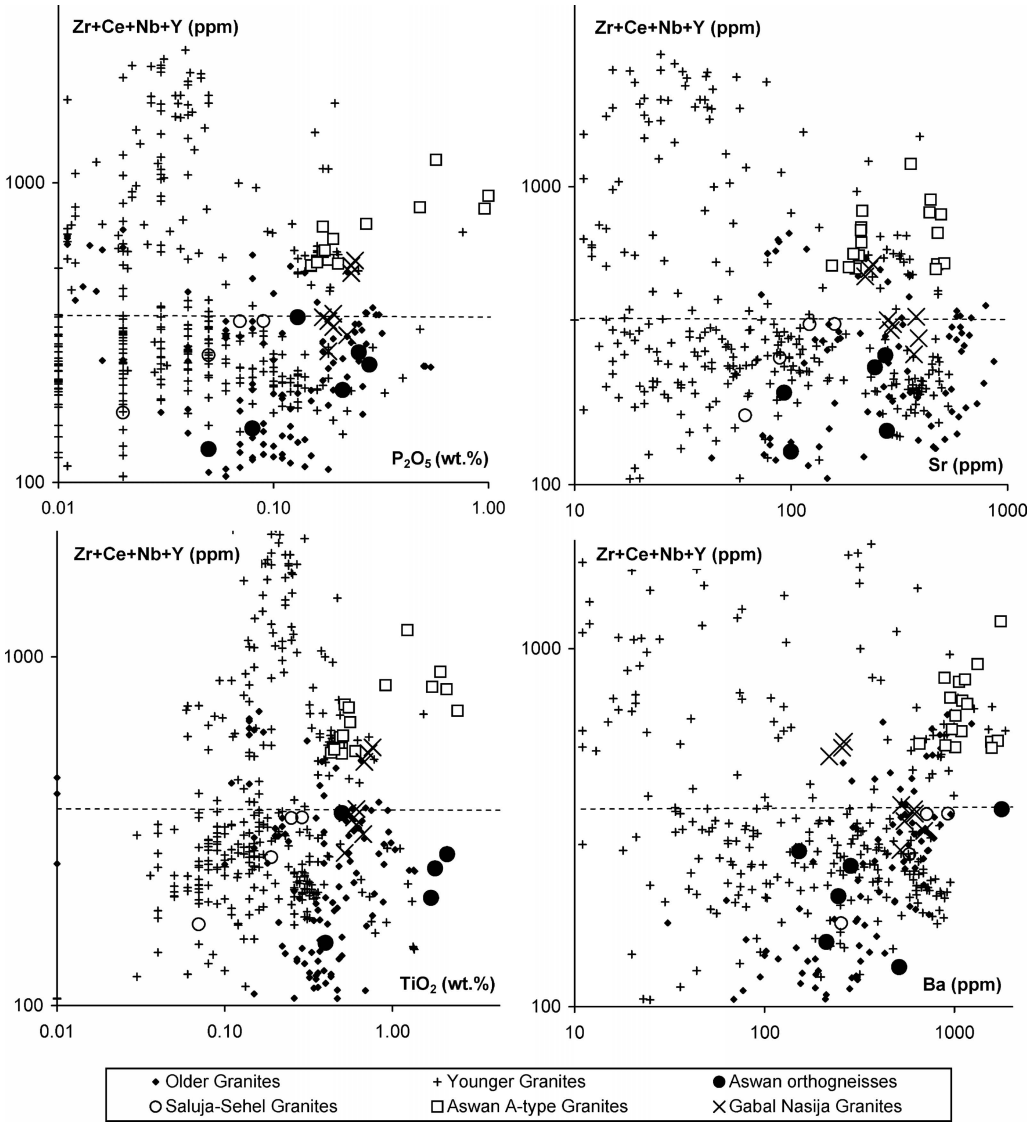

Fig. 8. Diagrams illustrating the particularly P, Ti, Sr and Ba-rich nature of the Aswan A-type granites in comparison to most other A-type granites of the Arabian Nubian Shield. Plots above dashed line ($Zr + Ce + Nb + Y = 350$ ppm) represent A-type granites according to Fig. 7b

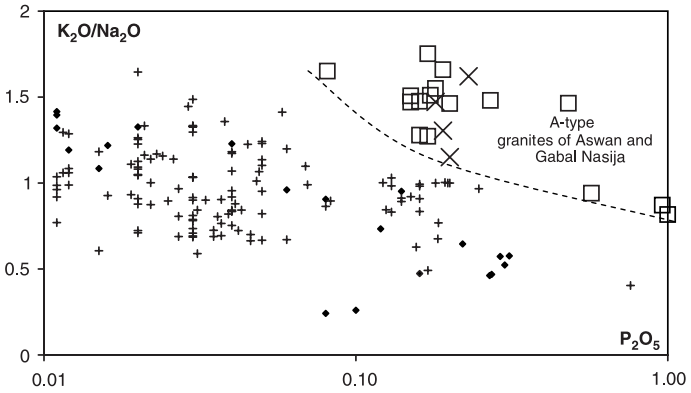

Fig. 9. Discrimination of the A-type granites of the Arabian Nubian Shield according to their K_2O/Na_2O ratios and P contents. Plotted are only granites with $Zr + Ce + Nb + Y > 350$ ppm. Symbols as in Fig. 8

tant to note that the bulk of A-type granites in the Arabian Nubian Shield do not show the high Sr, Ba, P and Ti contents of the Aswan A-type granites (Fig. 8). We found only a few other granites in the database (Table 4) that displayed both high Zr and LREE contents and high Sr, Ba, P *and* Ti contents. These examples include G1 granites from Gebel Abu El Hassan and Gebel St. Katharina (Dawoud, 1995; Gharib and Obeid, 2004) and younger granites from Abu Marva (El Mahallawi, 1989). However, even in these cases a clear chemical distinction from the Aswan A-type granites is provided by the K_2O/Na_2O ratios (Fig. 9). Thus, from the viewpoint of geochemistry, the Aswan A-type granites can be regarded as fairly unique within the large granite terrain of the Arabian Nubian Shield. HFSE-enriched variants of rapakivi granites from Gabal Nasija, ca. 200 km SSE of Aswan (El-Tokhi and Saleh, 2001), show the relatively closest similarities with the Aswan A-type granites. However, their Ba contents are somewhat lower (Fig. 8).

Discussion and conclusions

Geological significance of the new geochronological data

The zircon formation ages of 606 ± 2 Ma and 606 ± 1 Ma calculated in this study for the Monumental Granite and the Aswan Tonalite on the basis of U-Pb ID-TIMS analyses can be regarded as reliable, because they refer to concordant low-error data points. Due to the post-tectonic setting of both plutonic units (Gindy and Tamish, 1998), it can be concluded that the collision between the Arabian Nubian Shield and the Saharan Metacraton (West Gondwana) occurred prior to 606 ± 1 Ma in the Aswan area.

The zircon age of 622 ± 11 Ma for the tonalitic gneiss, and the presence of exclusively Neoproterozoic inherited zircon components in all granitoids, confirm that the metamorphic complex at Aswan is not a reworked part of the Saharan Metacraton. Gindy and Tamish (1998) proposed that the metamorphic complex formed when sedimentary and magmatic Arabian Nubian Shield material was

accreted against the Saharan Metacraton. If this is the case, then the maximum possible age for the collision event is indicated by the formation ages of the deformed granitic (tonalitic) gneisses. Sultan et al. (1994) have obtained an upper intercept age of 634 ± 4 Ma for one of these orthogneisses from Aswan City, which is fairly close to our tonalite gneiss age. For a granitic gneiss from Gebel um Shagir, ca. 100 km SW of Aswan, Sultan et al. (1994) published a similar zircon age of 626 ± 4 Ma (upper intercept). These ages are all relatively young when compared to other orthogneiss and metagranite occurrences in the Arabian Nubian Shield. Geochronological data for these are mostly between 680 and 850 Ma (Kröner et al., 1994; Stern and Abdelsalam, 1998). Thus, a relatively young magmatic arc (~ 630 Ma) seems to have existed at the western margin of the Arabian Nubian Shield, whereas remnants of older island arcs (amalgamated prior to 630 Ma) are present farther east (cf. Stoeser and Camp, 1985; Stern and Abdelsalam, 1998).

It is unfortunate that there are no geochronological data available for the metamorphic minerals (biotite, hornblende and monazite) of the Aswan gneiss complex. Such data could probably provide much better age constraints for the collision event. Finger and Helmy (1998) dated monazite from paragneisses from Abu Swayel, ca. 200 km SSE of Aswan at 636 ± 10 Ma and 633 ± 10 Ma. These are relatively imprecise electron microprobe ages. However, if these ages and errors are correct, then crustal thickening at the western margin of the Eastern Desert should have occurred prior to ~ 620 Ma. Similarly, Greiling et al. (1994) proposed, based on structural data, that at 615 Ma processes of compression and crustal shortening in the Arabian Nubian Shield were generally over and superseded by strike-slip tectonics. A phase of medium-pressure metamorphism in the Sinai, considered related to the collision of East- and West Gondwana, was inferred to have occurred at 620 ± 10 Ma (Cosca et al., 1999). Based on the age of a syntectonic granite in the Meatiq Dome, Stern and Hedge (1985) suggested that major crustal movements in the central Eastern Desert occurred at ca. 615 Ma. According to Fritz et al. (2002), these ca. 615 Ma old crustal movements in the Meatiq Dome were already extensional and post-dated an earlier accretionary phase.

As shown in this brief review, there seems to be a broad agreement in previous studies that the Arabian Nubian Shield was accreted to the Saharan Metacraton prior to 615 Ma and most probably between 615 and 630 Ma. If this is true, then the Aswan plutonic complex formed ca. 10–20 Ma after the collision. On the other hand, it is important to note that the Aswan Tonalite and the Monumental Granite are older than the bulk of ''younger granites'' in the Eastern Desert (600–550 Ma). The end of magmatic activity in the Aswan granite terrain is not well constrained due to the relatively large error in the age determination for the High-Dam Granite (595 ± 11 Ma) and the lack of age data for the Saluja-Sehel Granites. Although both are considered as younger than the Monumental Granite, based on field contacts, the actual time difference may have been small.

Magmatic processes

The oldest magmatic rocks in the study area, the orthogneisses, most probably represent magmas that formed immediately before the collision stage in a subduc-

tion environment. With one exception (sample RT-Z-7 of Sultan et al., 1994), these rocks have typical I-type (VAG) compositions like most of the pre-610 Ma granitoids in the Arabian Nubian Shield. Classical models of magma formation above subduction zones may therefore be suitable for explaining their petrogenesis. Such models involve mantle melting triggered by water introduction from the slab, formation of variably LIL-element-enriched basaltic melts, and development of more evolved dioritic, tonalitic, granodioritic and granitic melts via fractional crystallization (Pearce et al., 1984) and perhaps wall-rock assimilation (DePaolo, 1981).

On the other hand, it cannot be ruled out that some of the orthogneisses at Aswan (especially the high-K_2O and/or silicic ones) represent remelting products of older (meta)igneous crust (Chappell and White, 1974), bearing in mind that crustal growth in the Arabian Nubian Shield began as early as ca. 900 Ma (Kröner et al., 1990) and that the crust may have already had a considerable thickness at 630 Ma. The dated tonalitic orthogneiss (a high-K_2O-type) can be shown to contain appreciable amounts of inherited zircons derived from older Neoproterozoic crust. These zircons indicate either strong crustal contamination of a mantle-derived melt or the remelting of a crustal source.

Regarding the post-tectonic plutonism at Aswan, Gindy and Tamish (1998) concluded from their field observations that the Aswan Tonalite (named granodiorite by these authors), the Monumental Granite and the Saluja-Sehel Granites intruded within a relatively short time span along a N-S oriented conduit. Considering the new age information provided in the present paper, it appears likely that the plutonic events occurred within the frame of the transtensional-transpressional, broadly north-south directed strike-slip movements, which are documented for that time at many places in the Eastern Desert (Fritz et al., 2002; El Shafei and Kusky, 2003) as well as in the adjacent Saharan Metacraton (Abdelsalam et al., 2002, 2003).

Field relationships indicate that the formation of the composite plutonic complex began with the intrusion of the Aswan Tonalite. Judging from its shoshonitic affinities, this magma evolved from a mantle magma that formed by low-degree melting of an enriched, phlogopite-bearing mantle source. Cr, Ni and Co values are relatively low. Therefore, it is possible that a first stage of fractional crystallization occurred at mantle depth and that the primary magma was more mafic. The alternative possibility, namely derivation of the Aswan Tonalite from mafic lower crust, would require a highly unusual lower crustal source composition and is therefore considered less likely.

A genetic kinship between the Aswan Tonalite, the Monumental Granite and the High-Dam Granite is evident from their corresponding A-type nature. However, simple fractional crystallization models cannot sufficiently explain the data distributions seen in geochemical diagrams. Models involving source heterogeneities, magma mixing or wall rock assimilation are required to describe the plutonic evolution. The late Saluja-Sehel Granite shows features of I-type granites and may be derived from an igneous (arc-type) lower crustal source. A detailed assessment of the obviously complex magma forming processes is clearly beyond the scope of this paper and would need more sampling and a comprehensive geochemical study involving isotopes.

Tectonic implications

It is interesting to discuss the tectonic scenario that led to the shoshonitic A-type plutonism at Aswan and why granitoids emplaced in the Aswan area are geochemically distinct from most other granitoids in the Eastern Desert. Obviously, the source rocks and the magma forming processes must have been special at Aswan. As mentioned above, the only correlatives to the Aswan A-type granites yet known in Egypt are granites from Gabal Nasija, which is some 200 km SSE of Aswan. Notably, this area also lies near the inferred suture between the Arabian Nubian Shield and the Saharan Metacraton (Fig. 1). It is therefore reasonable to speculate that the petrogenesis of the Aswan A-type granites (and those at Gabal Nasija) is related to special geological circumstances in the proximity of this suture zone. Note that, for instance, broadly coeval granites farther east such as at Abu Ziran (614 ± 8 Ma, Stern and Hedge, 1985), which are considered as belonging to the ''older grey granites'', are clearly different and display I-type characteristics (El-Mahallawi and Berczi, 1989).

A first idea would be to examine whether the source material near the suture could reflect involvement of old lithosphere of the Saharan Metacraton at depth. However, such a model receives no support from isotopic data ($^{87}Sr/^{86}Sr$ initial ratios; ages of inherited zircon – see above) and is particularly at variance with the available Nd isotope data for the Monumental Granite. A recalculation of the +2.3 (T = 680 Ma) εNd value given in Harris et al. (1984) and the +1 (T = 594 Ma) εNd value given in Sultan et al. (1990) with the new 606 Ma intrusion age for the Monumental Granite results in εNd_i values of +1.4 and +1.1, respectively. This is on the lower end of the εNd_i spectrum known for granitoid rocks from the Arabian Nubian Shield (+1 to +5; Stern and Kröner, 1993; Moghazi et al., 1998; Moghazi, 1999), but still significantly above values of −5 to −11 reported for Late Neoproterozoic intrusions west of the Nile, that penetrate metacratonic crust (Harms et al., 1990). Had the LREE enrichment recorded in the Monumental Granite ($Sm/Nd \sim 0.16$) been inherited from a Palaeoproterozoic source, the εNd (T = 606) values would be inevitably much less radiogenic than +1.

Phlogopite-bearing and LILE and HFSE enriched reservoirs in the mantle, which are the most commonly presumed sources of shoshonitic magmatism, normally form above subduction zones (e.g., Fitton et al., 1991; Hawkesworth et al., 1995; Wilson et al., 1997), even though melting of such enriched mantle often occurs in a post-collisional setting (Vaisanen et al., 2000; Miller et al., 2003; Anderson et al., 2006; Jiang et al., 2006). There is little information in the published literature about the position and geometry of subduction zones in the Arabian Nubian Shield. Abdel Rahman (1995) suggested that, at ca. 600 Ma, the Arabian Nubian Shield was a continental-arc terrane at the margin of the Saharan Metacraton, under which oceanic crust was subducted in a continentward, that is westward, direction. However, there is also the possibility that the subduction polarity was eastward, i.e., that remnants of the Mozambique ocean (Kusky et al., 2003) were subducted eastwards below the Arabian Nubian Shield. Our model in Fig. 10 attempts to illustrate this situation. Eastward directed subduction processes could explain both the formation of a metasomatized and crustal-contaminated mantle wedge close to the plate edge and the ca. 630 Ma old volcanic arc magmatism recorded in the Aswan ortho-

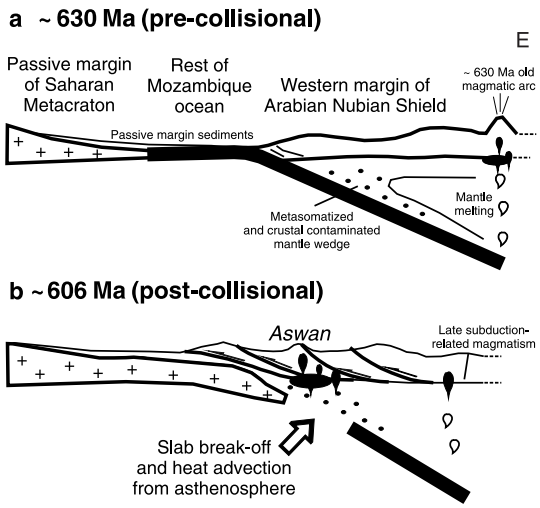

Fig. 10. Model showing the possible relations between tectonic and magmatic processes at the contact of the Saharan Metacraton and the Arabian Nubian Shield (see text for explanations)

gneisses. The generally observed westward thrusting of nappes (Habib et al., 1983; Gindy and Tamish, 1998) could be interpreted in terms of a Late Neoproterozoic accretionary wedge (pro-wedge). Our model is not necessarily at variance with the work of Fritz et al. (2002), who proposed that parts of the Eastern Desert were in extension from about 660 Ma onwards. It is feasible that compressional tectonics, related to the collision between the Saharan Metacraton and the Arabian Nubian Shield, was only severe in a relatively small zone along the western margin of the Eastern Desert.

In order to explain why the presumed shoshonitic mantle source began to melt ca. 10–20 Ma after the onset of collision, we advocate here a model of slab break-off (Von Blankenburg and Davis, 1995). This process involves a sudden introduction of heat from the asthenospheric mantle to the metasomatized mantle wedge above the subduction zone and would cause this metasomatized mantle to melt. As can be seen in Fig. 10, we suggest that slab break-off prohibited a further eastward descent of the cratonic lower plate and that no cratonic crust of the Saharan Metacraton underlies the area of Aswan. Since the inherited zircon age spectrum in the granitoids appears to be essentially Neoproterozoic and not Palaeoproterozoic, we see no reason to assume that pre-Neoproterozoic crust underlies this area. Nevertheless, we consider it possible, and even likely, that the magmas may have contained minor ''cratonic components'', as suggested by Sultan et al. (1992) on the basis of Pb isotope ratios from K-feldspar. These could have been imported into the upper plate via fluids derived from subducted passive margin sediments (Fig. 10).

Slab break-off is generally considered to produce relatively thin and orogen-parallel, linear thermal anormalies in the mantle, but no large-scale heating of the lithosphere (Von Blankenburg and Davis, 1995). Therefore, and because of the time difference between the events, a slab break-off process as suggested in Fig. 10 can hardly be made responsible for the widespread and voluminous granite-forming processes that occurred between ca. 600 and 550 Ma almost everywhere in the Eastern Desert. Also, there is broad agreement that subduction zones were no longer active at that time in the Arabian Nubian Shield. Following the published

literature (Table 4), it should have been mainly the remelting of subcontinental lithospheric mantle and island-arc-type lower crust, that supplied the magmas during this time span. This requires large-scale heat introduction from the asthenospheric mantle, which may have occurred in an environment of post-collisional streching of the lithosphere (Stern et al., 1984).

Acknowledgements

This paper benefited from comments by H. Fritz, A. Kröner, A. Möller and R. Stern. Thanks also to Gudrun Riegler for her tireless assistance during the preparation of text and figures, and Malcolm Roberts for linguistic manuscript improvements.

References

Abdel Monem AA, Hurley PM (1980) Age of Aswan monumental granite, Egypt, by U-Pb dating of zircon. Bulletin of the institute of applied geology. King Abdel Aziz University Jeddah 3: 141–144

Abdel-Rahman AFM (1995) Tectonic-magmatic stages of shield evolution: the Pan-African belt in northeastern Egypt. Tectonophysics 242: 223–240

Abdel-Rahman AM, Martin RF (1990) The Mount Gharib A-type granite, Nubian Shield: petrogenesis and role of metasomatism at the source. Contrib Mineral Petrol 104: 173–183

Abdelsalam MG, Liégeois JP, Stern RJ (2002) The Saharan metacraton. J Afr Earth Sci 34: 119–136

Abdelsalam MG, Abdel-Rahman EM, El-Faki EM, Al-Hur B, El-Bashier FM, Stern RJ, Thurmond AK (2003) Neoproterozoic deformation in the northeastern part of the Saharan Metacraton, northern Sudan. Precamb Res 123: 203–221

Ahmed AF, El-Mahallawi MM (1995) Petrology, geochemistry and petrogenesis of some granitoid rocks from the northern and central eastern desert, Egypt. Egypt J Geol 39: 739–767

Anderson UB, Eklund O, Fröjdö S, Konopelko D (2006) 1.8 Ga magmatism in the Fennoscandian shield; lateral variations in subcontinental mantle enrichment. Lithos 86: 110–136

Bonin B (1992) The role of crust in the development of A-type alkali-feldspar granites in within-plate bimodal alkaline magmatism. Ind Geol Assoc Bull 25: 11–27

Bregar M, Bauernhofer A, Pelz K, Kloetzli U, Fritz H, Neumayr P (2002) A late neoproterozoic magmatic core complex in the eastern desert of Egypt: emplacement of granitoids in a wrench-tectonic setting. Precamb Res 118: 59–82

Chappell BW, White AJR (1974) Two contrasting granite types. Pac Geol 8: 173–174

Chappell BW, Byant CJ, Wyborn D, White AJR, Williams IS (1998) High- and low-temperature I-type granites. Resour Geol 48: 225–235

Clemens JD, Vielzeuf D (1987) Constraints on melting and magma production in the crust. Earth Planet Sc Lett 86: 287–306

Collins WJ, Beams SD, Chappell BW, White AJR (1982) Nature and origin of A-type granites with particular reference to south-eastern Australia. Contrib Mineral Petrol 80: 189–200

Cosca MA, Shimron A, Caby R (1999) Late Precambrian metamorphism and cooling in the Arabian-Nubian Shield: petrology and $^{40}Ar/^{39}Ar$ geochronology of metamorphic rocks of the Elat area (southern Israel). Precamb Res 98: 107–127

Dawoud M (1995) Petrography, geochemistry and tectonic environment of the granitic rocks of Gebel Abu El Hassan-Gebel Abu Samyuk, Northern Eastern Desert, Egypt. Thesis, 157 pp

DePaolo DJ (1981) Trace element and isotopic effects of combined wallrock assimilation and fractional crystallization. Earth Planet Sci Lett 53: 189–202

Dixon TH, Golombek MP (1988) Late Precambrian crustal accretion rates in northeast Africa and Arabia. Geology 16: 991–994

El-Gaby S (1975) Petrochemistry and geochemistry of some granites from Egypt. N Jahrb Mineral Abh 124: 147–189

El-Gaby S, List FK, Tahrani R (1990) The basement complex of the Eastern Desert and Sinai. In: Said R (ed) The geology of Egypt. Balkema Rotterdam, Netherlands, pp 175–184

El-Mahallawi MM (1989) Petrology and geochemistry of some granitic rocks from the central eastern desert, Egypt. Egypt J Geol 33: 47–69

El-Mahallawi MM (1995) Rare earth elements geochemistry and petrogenesis of the Shaitian granitoid rocks, Wadi Shait area, Eastern Desert, Egypt. Sci Bull El-Minia Univ 8: 79–96

El-Mahallawi MM, Berczi J (1989) Geochemistry of rare earth elements and petrogenesis of some Egyptian granites. Sci Bull El-Minia Univ 2: 155–176

El-Metwally AA (1997) Origin and emplacement of a reversely zoned Pan-African granitoid pluton from the Sinai Massif, Egypt. J Afr Earth Sci 24: 29–38

El-Ramly MF, Akaad MK (1960) The basement complex in the central eastern desert of Egypt between latitudes 24°30′ and 25°40′ N. Geological survey of Egypt, Cairo, Paper 8, 35 pp

El-Sayed MM, Mohamed FH, Furnes H, Kanisawa S (2002) Geochemistry and petrogenesis of the neoproterozoic granitoids in the central eastern desert, Egypt. Chem Erde 62: 317–346

El-Sayed MM, Mohamed FH, Furnes H (2004) Petrological and geochemical constraints on the evolution of late Pan-African Bakriya post-orogenic ring complex, Central Eastern Desert, Egypt. N Jahrb Mineral Abh 180: 1–32

El-Shafei MK, Kusky TM (2003) Structural and tectonic evolution of the Neoproterozoic Feiran-Solaf metamorphic belt, Sinai Peninsula: implications for the closure of the Mozambique Ocean. Precamb Res 123: 269–293

El-Tokhi MM, Saleh GM (2001) The evolution of Pan African Aswan-type Rapakivi granite, geochemical evidences from the south eastern desert of Egypt. Egypt J Geol 45: 295–307

Finger F, Helmy HM (1998) Composition and total-Pb model ages of monazites from high-grade paragneisses in the Abu Swayel area, southern eastern desert, Egypt. Mineral Petrol 62: 269–289

Fitton JG, James D, Leeman WP (1991) Basic magmatism associated with late Cenozoic extension in the western United States: compositional variations in space and time. J Geophys Res 96: 13693–13711

Fritz H, Dallmeyer DR, Wallbrecher E, Loizenbauer J, Hoinkes G, Neumayr P, Khudeir AA (2002) Neoproterozoic tectonothermal evolution of the Central Eastern Desert, Egypt: a slow velocity tectonic process of core complex exhumation. J Afr Earth Sci 34: 137–155

Gerdes A, Zeh A (2006) Combined U-Pb and Hf isotope LA-(MC-)ICP-MS analyses of detrital zircons: comparison with SHRIMP and new constraints for the provenance and age of an Armorican metasediment in central Germany. Earth Planet Sci Lett 249: 47–61

Gharib ME, Dawoud M (2005) Inheritance in zircon from Aswan granitoids: the role of contamination at the western boundary of the Nubian Shield. First International Conference on the Tethys, Cairo University, pp 11–28

Gharib ME, Obeid MA (2004) Geochemistry and evolution of the Neoproterozoic granitoid magmatism in the Wadi El-Sheikh-Gabal Saint Katherina area, Southwestern Sinai, Egypt. Proc. 7th Int. Conf. on the Geology of the Arab World, Cairo University, pp 53–73

Ghoneim MF, Hassan AM, Abu Anbar MM (1999) Post-orogenic and rift-related ring complexes in Egypt: geochemical and isotopic discrimination. International Conference on the Geology of the Arab World, Cairo University, pp 246–265

Gindy AR (1956) The igneous and metamorphic rocks of the Aswan area, with a new geological exposure-map (scale 1:10000). Bulletin de l'Institute d'Egypt 37: 83–120

Gindy AR, Tamish MM (1998) Petrogenetic revision of the basement rocks in the environs of Aswan, southern Egypt. Egypt J Geol 42: 1–14

Greiling RO, Abdeen MM, Dardir AA, El Akhal H, El Ramly ME, Kamal El Din GM, Osman AF, Rashwan AA, Rice AHN, Sadek MF (1994) A structural synthesis of the Proterozoic Arabian-Nubian Shield in Egypt. Geol/Rundsch 83: 484–501

Habib ME, El-Gaby S, Ghazaly M (1983) Tectonic history of El-Hudi Nappe, East of Aswan, Egypt. 5th International Conference on Basement Tectonics. Cairo University, Abstract volume, 27 pp

Harms U, Schandelmeier H, Darbyshire DPF (1990) Pan-African reworked early/middle Proterozoic crust in NE Africa west of the Nile: Sr and Nd isotope evidence. J Geol Soc London 147: 859–872

Harris NBW, Hawkesworth CJ, Ries AC (1984) Crustal evolution in north-east and east Africa from model Nd ages. Nature 309: 773–776

Hashad AH, Sayyah TA, El Koly SB, Youssif A (1972) Rb/Sr isotopic age determinations of some basement Egyptian granites. J Geol 16: 296–281

Hassan MA, Hashad AH (1990) Precambrian of Egypt. In: Said R (ed) The geology of Egypt. Balkema, Rotterdam, Netherland, pp 201–248

Hassan MA, Abu Anbar MM (1997) Geochemistry and mineral chemistry of some alkalic granites of Egypt. The Third Conference on Geochemistry, Alexandria, Egypt, pp 121–137

Hawkesworth C, Turner S, Gallagher K, Hunter A, Bradshaw T, Rogers N (1995) Calc-alkaline magmatism, lithospheric thinning and extension in the Basin and range. J Geophys Res 100: 10271–10286

Hussein AA, Ali MM, El-Ramly MF (1982) A proposed new classification of the granites of Egypt. J Volcan Geothermal Res 14: 187–198

Jackson NJ, Walsh JN, Pegram E (1984) Geology, geochemistry and petrogenesis of late Precambrian granitoids in the central Hijaz region of the Arabian shield. Contrib Mineral Petrol 87: 205–219

Janousek V, Gerdes A, Vrana S, Finger F, Erban V, Friedl G, Braithwaite CJR (2006) Low-pressure granulites of the Lisov Massif, southern Bohemia: Visean metamorphism of late Devonian plutonic arc rocks. J Petrol 47: 705–744

Jiang YH, Jiang SY, Ling HF, Dai BZ (2006) Low-degree melting of a metasomatized lithospheric mantle for the origin of Cenozoic Yulong monzogranite-porphyry, east Tibet: geochemical and Sr-Nd-Pb-Hf isotopic constraints. Earth Planet Sci Lett 241: 617–633

Krogh TE (1973) A low contamination method for hydrothermal decomposition of zircon and extraction of U and Pb for isotopic age determinations. Geochim Cosmochim Acta 37: 485–494

Krogh TE (1982) Improved accuracy of U-Pb ages by the creation of more concordant systems using an air abrasion technique. Geochim Cosmochim Acta 46: 637–649

Kröner A (1985) Ophiolites and the evolution of tectonic boundaries in the Late Proterozoic Arabian-Nubian shelf of NE Africa and Arabia. Precamb Res 27: 277–300

Kröner A, Eyal M, Eyal Y (1990) Early Pan-African evolution of the basement around Elat, Israel, and the Sinai Peninsula revealed by single-zircon evaporation dating, and implications for crustal accretion rates. Geology 18: 545–548

Kröner A, Krüger J, Rashwan AAA (1994) Age and tectonic setting of granitoid gneisses in the eastern desert of Egypt and south-west Sinai. Geol Rundsch 83: 502–513

Kusky TM, Abdelsalam M, Tucker R, Stern R (2003) Evolution of the East African and related orogens, and the Assembly of Gondwana. Precamb Res 123: 81–85

Leggo PJ (1968) Some recent isotopic investigations. Annual Report of the Research Institute for African Geology, Leeds University, Vol 12, pp 45–46

Ludwig KR (1988) PBDAT for MS-DOS: a computer program for IBM-PC compatibles for processing raw Pb-U-Th isotope data: OF 88-0542, U.S. Geological Survey Open-File Report

Ludwig KR (2000) Users manual for isoplot/ex rev.2.49: a geochronological toolkit for Microsoft excel. Berkeley Geochronology Center, Special Publication, v. 1a, pp 1–56

Miller C, Schuster R, Klötzli U, Frank W, Purtscheller F (2003) Post-collisional potassic and ultrapotassic magmatism in SW Tibet: geochemical and Sr-Nd-Pb-O isotopic constraints for mantle source characteristics and petrogenesis. J Petrol 40: 1399–1424

Moghazi AM (1999) Magma source and evolution of Late Neoproterozoic granitoids in Gabal El-Urf area, eastern desert, Egypt: geochemical and Sr-Nd isotopic constraints. Geol Mag 136: 285–300

Moghazi AM (2002) Petrology and geochemistry of Pan-African granitoids, Kab Amiri area, Egypt – implications for tectonomagmatic stages in the Nubian Shield evolution. Mineral Petrol 75: 41–67

Moghazi AM, Andersen T, Oweiss GA, El Bouseily AM (1998) Geochemical and Sr-Nd-Pb isotopic data bearing on the origin of Pan-African granitoids in the Kid area, southeast Sinai, Egypt J Geol Soc 155: 697–710

Noweir AM, Abu El Ela AM, Sewifi BM (1990) New contributions to the geology, geochemistry and tectonic setting of the Aswan granites, southern Egypt. Qatar Univ Sci Bull 10: 395–419

Parrish RR (1987) An improved micro-capsule for zircon dissolution in U-Pb geochronology. Chem Geol 66: 99–102

Pearce JA, Harris NBW, Tindle AG (1984) Trace element discrimination diagrams for the tectonic interpretation of granitic rocks. J Petrol 25: 956–983

Pecerillo A, Taylor SR (1976) Geochemistry of Eocene calc-alkaline volcanic rocks from the Kastamonu area, northern Turkey. Contrib Mineral Petrol 58: 63–81

Ragab AI, Meneisy MY, Taher RM (1978) Contributions of the petrogenesis and age of Aswan granitic rocks, Egypt. N Jahrb Mineral Abh 133: 71–87

Schandelmeier H, Kuster D, Wipfler E, Abdel Rahman EM, Stern RJ, Abdelsalam MG, Sultan M (1993) Evidence for a new late Proterozoic suture in northern Sudan. In: Thorweihe U, Schandelmeier H (eds) Geoscientific research in Northeast Africa. Balkema, Rotterdam, pp 83–85

Stacey JS, Kramers JD (1975) Approximation of terrestrial lead isotope evolution by a two-stage model. Earth Planet Sci Lett 26: 207–221

Stern RJ, Hedge CE (1985) Geochronologic and isotopic constraints on late Precambrian crustal evolution in the eastern desert of Egypt. Am J Sci 285: 97–127

Stern RJ, Kröner A (1993) Late Precambrian crustal evolution in NE Sudan: isotopic and geochronologic constraints. J Geol 101: 555–574

Stern RJ, Abdelsalam MG (1998) Formation of juvenile continental crust in the Arabian-Nubian Shield: evidence from granitic rocks of the Nakasib suture, NE Sudan. Geol Rundsch 87: 150–160

Stern RJ, Gottfried D, Hedge CE (1984) Late Precambrian rifting and crustal evolution in the northeastern desert of Egypt. Geology 12: 168–172

Stoeser DB, Camp VE (1985) Pan African microplate accretion of the Arabian Shield. Geol Soc Am Bull 96: 817–826

Sultan M, Chamberlain KR, Bowring SA, Arvidson RE, Abuzied H, El Kaliouby B (1990) Geochronological and isotopic evidence for involvement of pre-Pan-African crust in the Nubian Shield, Egypt. Geology 18: 761–764

Sultan M, Bickford ME, El Kaliouby B, Arvidson RE (1992) Common Pb systematics of Precambrian granitic rocks of the Nubian Shield (Egypt) and tectonic implications. Geol Soc Am Bull 104: 456–470

Sultan M, Tucker RD, El Alfy Z, Attia R, Ragab AG (1994) U-Pb (zircon) ages for the gneissic terrane west of the Nile, southern Egypt. Geol Rundsch 83: 514–522

Vaisanen M, Manttari I, Kriegsman LM, Holtta P (2000) Tectonic setting of post-collisional magmatism in the Palaeoproterozoic Svecofennian Orogen, SW Finland. Lithos 54: 63–81

Von Blankenburg F, Davis JH (1995) Slab breakoff: a model for syncollisional magmatism and tectonics in the Alps. Tectonics 14: 120–131

Watson EB, Harrison TM (1983) Zircon saturation revisited: temperature and composition effects in a variety of crustal magma types. Earth Planet Sci Lett 64: 295–304

Whalen JB, Currie KL, Chappel BW (1987) A-type granites: geochemical characteristics, discrimination and petrogenesis. Contrib Mineral Petrol 95: 407–419

Wilson M, Tankut A, Gulec N (1997) Tertiary volcanism of the Galatia province, north-west central Anatolia, Turkey. Lithos 42: 105–121